



Article

Photohormones Enable Optical Control of the Peroxisome Proliferator-Activated Receptor Gamma (PPAR#)

Konstantin Hinnah, Sabine Willems, Johannes Morstein, Jan Heering, Felix Hartrampf, Johannes Broichhagen, Philipp Leippe, Daniel Merk, and Dirk Trauner

J. Med. Chem., **Just Accepted Manuscript** • DOI: 10.1021/acs.jmedchem.0c00654 • Publication Date (Web): 04 Sep 2020

Downloaded from pubs.acs.org on September 4, 2020

Just Accepted

"Just Accepted" manuscripts have been peer-reviewed and accepted for publication. They are posted online prior to technical editing, formatting for publication and author proofing. The American Chemical Society provides "Just Accepted" as a service to the research community to expedite the dissemination of scientific material as soon as possible after acceptance. "Just Accepted" manuscripts appear in full in PDF format accompanied by an HTML abstract. "Just Accepted" manuscripts have been fully peer reviewed, but should not be considered the official version of record. They are citable by the Digital Object Identifier (DOI®). "Just Accepted" is an optional service offered to authors. Therefore, the "Just Accepted" Web site may not include all articles that will be published in the journal. After a manuscript is technically edited and formatted, it will be removed from the "Just Accepted" Web site and published as an ASAP article. Note that technical editing may introduce minor changes to the manuscript text and/or graphics which could affect content, and all legal disclaimers and ethical guidelines that apply to the journal pertain. ACS cannot be held responsible for errors or consequences arising from the use of information contained in these "Just Accepted" manuscripts.

**Photohormones Enable Optical Control of the Peroxisome Proliferator-Activated
Receptor Gamma (PPAR γ)**

Konstantin Hinnah^{#a}, Sabine Willems^{#b}, Johannes Morstein^a, Jan Heering^c, Felix W. W.
Hartrampf^d, Johannes Broichhagen^d, Philipp Leippe^d, Daniel Merk^{*b}, Dirk Trauner^{*a,d}

a Department of Chemistry, New York University, New York, New York 10003, USA

b Institute of Pharmaceutical Chemistry, Goethe-University Frankfurt, Max-von-Laue-Strasse 9,
60438 Frankfurt, Germany

c Fraunhofer Institute for Molecular Biology and Applied Ecology IME, Branch for Translational
Medicine and Pharmacology TMP, Theodor-Stern-Kai 7, 60596 Frankfurt, Germany

d Department of Chemistry and Center for Integrated Protein Science (CIPSM), Ludwig-
Maximilians-University Munich, Butenandtstrasse 5-13, 81377 Munich, Germany

Abstract

Photopharmacology aims at the optical control of protein activity using synthetic photoswitches. This approach has been recently expanded to nuclear hormone receptors with the introduction of 'photohormones' for retinoic acid receptor, farnesoid X receptor and estrogen receptor. Herein, we report the development and profiling of photoswitchable agonists for peroxisome proliferator-activated receptor γ (PPAR γ). Based on known PPAR γ ligands (MDG548, GW1929 and Rosiglitazone) we have designed and synthesized azobenzene derivatives, termed **AzoGW1929** and **AzoRosi**, which were confirmed to be active in cell-based assays. Subsequent computer-aided optimization of **AzoRosi** resulted in the photohormone **AzoRosi-4** which bound and activated PPAR γ preferentially in its light-activated *cis*-configuration.

Introduction

Nuclear hormone receptors (NHRs) are ligand-inducible transcription factors that interact with specific DNA response elements to elicit a transcriptional response of their target genes.^{1,2} They control a wide variety of biological processes, ranging from cell proliferation and differentiation to metabolism, homeostasis and morphogenesis.³ This receptor class is modulated by a broad spectrum of endogenous molecules, including thyroid and steroid hormones, bile acids and fatty acids, retinoids and Vitamin D.⁴

Peroxisome proliferator-activated receptors (PPARs) belong to the class I subfamily of NHRs and comprise three isoforms (PPAR α , PPAR δ and PPAR γ), which exhibit different tissue localization.^{5,6} PPARs form a heterodimer with the retinoid X receptor (RXR), and upon-ligand binding they regulate transcription levels of genes involved e.g. in metabolic balance and inflammatory processes.⁷ The PPAR γ subtype is mainly expressed in adipose tissue but also found in the liver, heart, brain, and macrophages. It controls insulin secretion, lipid and glucose metabolism, and is considered the master regulator of adipogenesis.⁸ PPAR γ is linked to diverse pathological conditions, such as diabetes, cardiovascular disorders, Alzheimer's and Parkinson's disease, multiple sclerosis, stroke and cancer.^{9–14}

In photopharmacology, photoswitchable small molecules are used to control biological processes with light.^{15–18} This approach has proven to be especially successful with lipophilic or amphiphilic molecules that can control GPCRs, ion channels, enzymes, or biophysical aspects of lipids.^{19–26} Amphiphilic agonists of NHRs could therefore be ideally suited for this approach. This was first exemplified with a photoswitchable retinoic acid derivative targeting the retinoic acid receptor α (RAR α).²⁷ Subsequently, we developed a photohormone for the bile acid receptor FXR that allows for the optical control of gene regulation in liver cells. In addition, a photoswitchable estrogen receptor (ER) agonist was recently reported by Tsuchiya.^{28,29} Here, we disclose the development

of photohormones for PPAR γ , extending the reach of photopharmacology to another important member of the NHR superfamily.

Results and Discussion

In our search for photoswitchable PPAR γ modulators, we screened various drug databases (DrugBank, PDB, ChEMBL, IUPHAR) for known PPAR γ modulators to identify promising chemotypes that could be modified with an azobenzene photoswitch. Molecules containing lipophilic segments that can be substituted with an azobenzene ('azologization') are particularly amenable to this approach.^{27,30} Most PPAR γ agonists share the common structure of fatty acid mimetics³¹ that are comprised of a polar, usually acidic, headgroup that engages in hydrogen bonding with the ligand-dependent activation function (AF-2), an aliphatic linker and a bulky aromatic tail that contributes to their function and potency (effector module).³² Based on these structural information, we envisioned that optical control over PPAR γ could be achieved by incorporation of an azobenzene photoswitch into the hydrophobic tail - a strategy that has been very successful for a number of bioactive lipids. Photoisomerization of the tail should lead to a steric clash in the ligand binding site that significantly decreases the affinity of one isomer to the receptor. Initial hits were further assessed based on previous SAR studies, crystal structure data, and molecular docking.³³⁻³⁷ Based on these considerations, we selected three chemotypes (MDG548, GW1929 and Rosiglitazone) as leads to develop PPAR γ -targeting photohormones (Figure 1).

The potential of the lead azolog scaffolds to act as photoswitchable PPAR γ ligands was studied by molecular docking. The X-ray complex structures of the PPAR γ ligand binding domain with bound Rosiglitazone (PDB ID: 5YCP³⁶) or GW1929 (PDB ID: 6D8X³⁷) served as templates. Structures were prepared and docking performed in the molecular operating environment (MOE). For each azolog, *cis*- and *trans*-isomer were individually docked and the resulting predicted binding modes were evaluated considering participation in the canonical H-bond network with the

PPAR γ activation triad His323, His449 and Tyr473, additional direct contacts to the binding site, absence or presence of clashes and similarity to the binding mode of the co-crystallized ligands. The design of candidate derivatives of **AzoGW1929** and **AzoRosiglitazone** was similarly supported by molecular docking to computationally assess their potential to act as optimized photohormones.

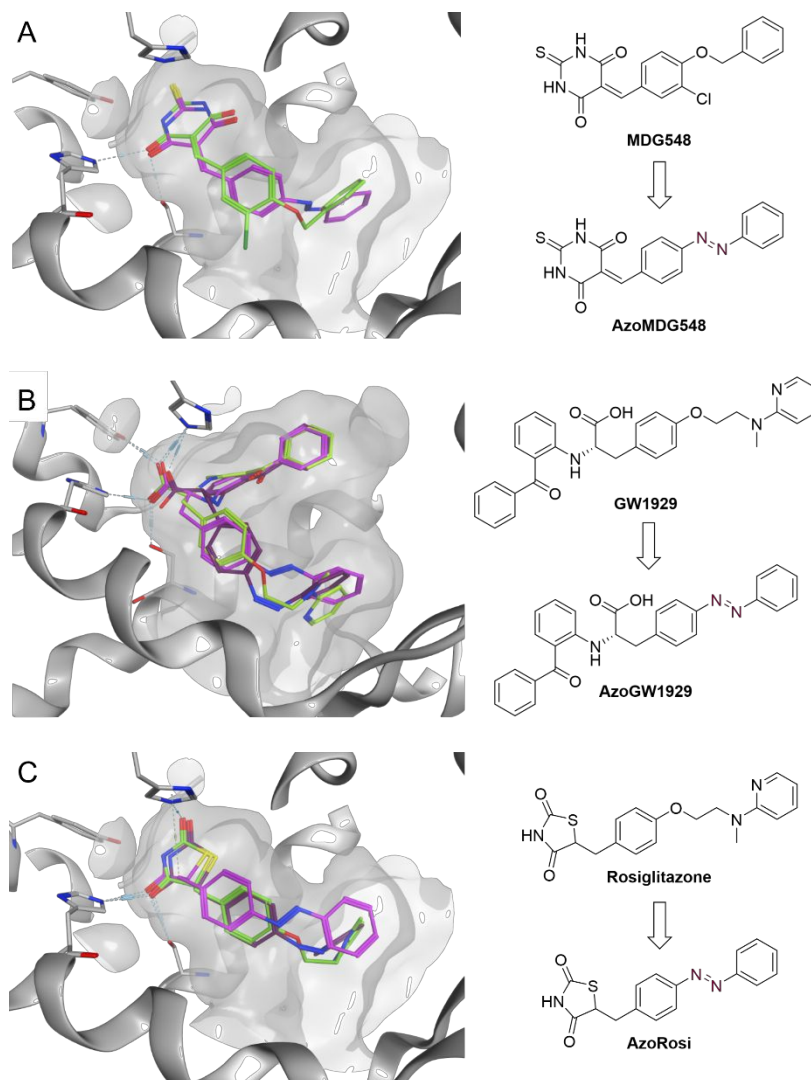


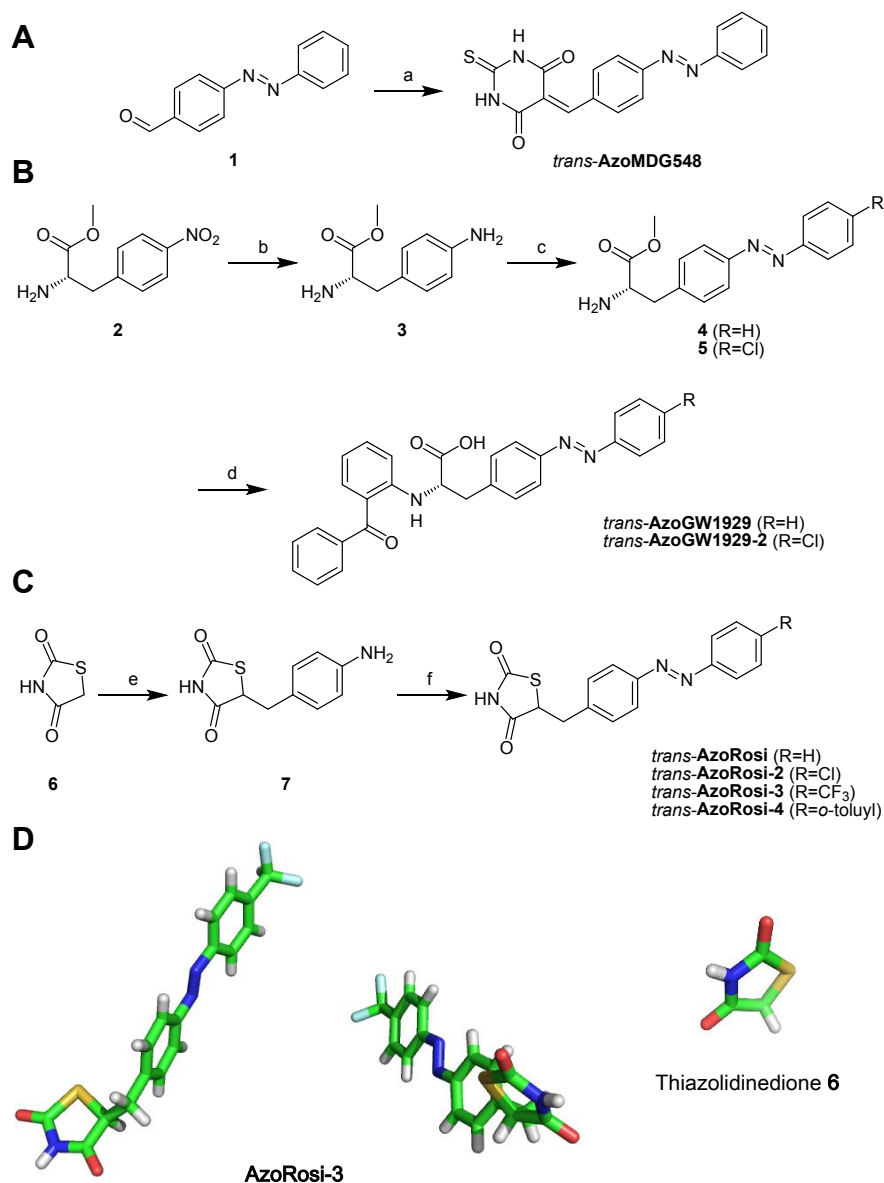
Figure 1. Molecular docking guides the design of photohormones for PPAR γ . Docking was performed in MOE³⁸ using X-ray crystal structures of PPAR γ complexed with the template ligands Rosiglitazone (A and C, green, PDB ID: 5YCP³⁶) and GW1929 (B, green, PDB ID:6D8X³⁷). (A) Incorporation of an azo group in MDG548 (green) to **AzoMDG548** (magenta) allowed minimal

changes to the structure. (B) In **AzoGW1929** (magenta), the azo group replaces the aminoethoxy linker of GW1929. (C) Azologization of Rosiglitazone by replacement of the aminoethoxy linker region (**AzoRosi**, magenta) resulted in favorable predicted binding modes of both (*cis*-/*trans*-) isomers.

AzoMDG548 (Figure 1A) was derived from the PPAR γ agonist MDG548 (EC_{50} = 215 nM)³⁵ featuring a benzyl phenyl ether moiety which is a common motif for azologization²⁷. The predicted binding mode of *trans*-**AzoMDG548** aligned well with the docked pose of MDG548 and with Rosiglitazone suggesting potential of the azolog for PPAR γ modulation. **AzoGW1929** was derived from the potent (EC_{50} = 1.47 nM) and selective PPAR γ agonist GW1929³⁹ (Figure 1B). Crystallographic data of the parent compound bound to PPAR γ showed that the benzophenone motif is bound in a lipophilic sub-pocket deep inside the ligand binding domain (LBD) (PDB ID: 6D8X) providing little space and flexibility for structural variation. Therefore, we reasoned that the aliphatic linker was more suitable for azologization. Docking studies on GW1929-derived azologs agreed with this hypothesis since predicted binding modes for analogs bearing the azo group in the benzophenone region did not align with the co-crystallized ligand but partly placed the designed structure outside the canonical binding pocket. In contrast, the predicted binding modes of **AzoGW1929**, where the azo motif replaces the aminoethoxy linker, aligned well with the co-crystallized ligand GW1929. Favorable poses were observed for both the *cis*- and *trans*-configuration of **AzoGW1929**, however. The preferred absolute configuration of GW1929 was retained in our azolog design and the (*S*)-enantiomer of **AzoGW1929** was prepared through an enantioselective synthesis.³² The clinically approved PPAR γ agonist Rosiglitazone⁴⁰ served as a template for our third azolog design. Multiple SAR studies demonstrate the importance of the thiazolidinedione headgroup and methylene linker of Rosiglitazone (EC_{50} = 43 nM)^{41,42} for potency. Therefore, we proposed to incorporate the azobenzene photoswitch into the hydrophobic tail of Rosiglitazone (Figure 1C). Docking of the azolog, termed **AzoRosi**, to a Rosiglitazone-bound PPAR γ crystal structure (PDB ID: 5YCP) resulted in favorable binding modes for both *cis*-

and *trans*-**AzoRosi** that aligned with the crystal bound template ligand and revealed participation in the canonical H-bond network with the activation triad (His323, His449, Tyr473).

The synthesis of **AzoMDG548** was achieved by coupling of 4-phenylazobenzaldehyde **1** to thiobarbituric acid via Knoevenagel-type condensation under reflux in ethanol (Scheme 1A). The synthesis route for **AzoGW1929** and derivative **AzoGW1929-2** started from (S)-4-nitrophenylalanine methyl ester hydrochloride **2** which was reduced to the corresponding amino compound using palladium on charcoal and hydrogen (Scheme 1B). Baeyer-Mills coupling of methyl (S)-2-amino-3-(4-aminophenyl)propanoate **3** with the corresponding aniline (unsubstituted aniline for **AzoGW1929** or 4-chloroaniline for **AzoGW1929-2**) and subsequent Buchwald-Hartwig cross coupling to the free amine of the amino acid afforded the methyl ester derivatives of the corresponding photohormones. Cleavage of the methyl esters with lithium hydroxide yielded **AzoGW1929** and **AzoGW1929-2**. Photoswitchable derivatives of Rosiglitazone (**AzoRosi**, **AzoRosi-2-4**) were obtained in four steps (Scheme 1C) starting with coupling of *para*-nitrobenzaldehyde to thiazolidinedione **6** in a Knoevenagel-type reaction. Two subsequent reduction steps with Hantzsch ester and palladium on charcoal under a hydrogen atmosphere gave 5-(4-aminobenzyl)thiazolidine-2,4-dione **7**. The final step comprised a Baeyer-Mills coupling with the corresponding (*para*-substituted) anilines to afford **AzoRosi** and derivatives **AzoRosi-2** to **AzoRosi-4**. The required aniline **9** for **AzoRosi-4** was synthesized in a Suzuki reaction from *para*-aminoboronic acid **8** and 2-bromotoluene (Scheme S1). The X-ray structure of the thiazolidinedione **6** and of *trans*-**AzoRosi-3** is shown in Scheme 1D.



Scheme 1. (A) a) thiobarbituric acid, EtOH, 80 °C, 2 h (46 %); (B) b) Pd/C, MeOH, rt, 16 h (quant.) c) i) aniline/4-chloroaniline, Oxone™, CH₂Cl₂, H₂O, rt, 16 h ii) **3**, MeOH, rt 16 h (70 % R=H, 34 % R=Cl) d) i) (2-bromophenyl)(phenyl)methanone, Cs₂CO₃, Pd(OAc)₂, BINAP, toluene, 110 °C, 3 h ii) LiOH, H₂O, ACN, rt, 3 h (56 % R=H, 31 % R=Cl over 2 steps); (C) e) i) 4-nitrobenzaldehyde, piperidine, AcOH, EtOH, μ w 150 °C, 20 min ii) Hantzsch ester, SiO₂, toluene, 110 °C, 20 h iii) Pd/C, MeOH, rt, 16 h (24 % over 3 steps) f) i) aniline/4-chloroaniline/4-trifluoromethylaniline/2'-methyl-[1,1'-biphenyl]-4-amine **9**, Oxone™, CH₂Cl₂, H₂O, rt, 16 h ii) **7**, MeOH, rt, 16 h (72 % R=H,

71 % R=Cl, 57 % R=CF₃, 49 % R=o-toluy) (D) Crystal structure of thiazolidinedione **6** and *trans*-**AzoRosi-3**.

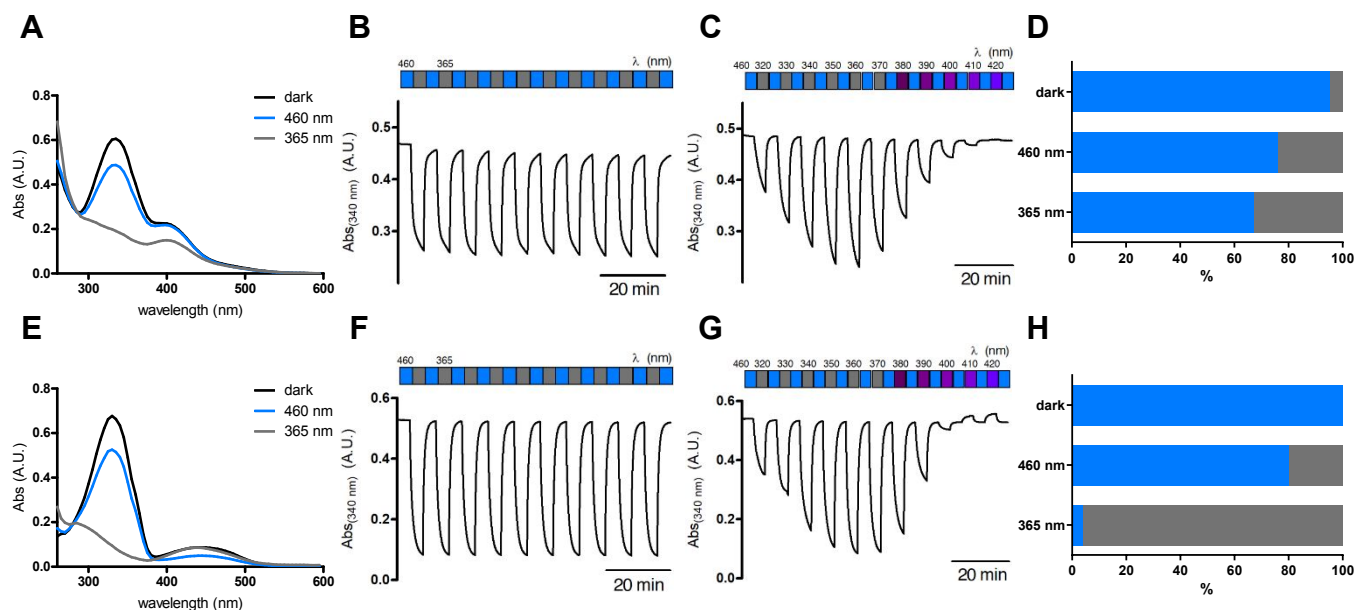


Figure 2. Photophysical evaluation. The UV-Vis spectra of **AzoGW1929** (A) and **AzoRosi** (E) (25 μ M in DMSO) in the dark-adapted (*trans*, black), 365 nm-adapted (*cis*, gray) and 460 nm-adapted (*trans*, blue) photostationary states. Reversible cycling of **AzoGW1929** (B) and **AzoRosi** (F) (25 μ M in DMSO) with alternating illumination at 365 nm and 460 nm. Reversible cycling between photoisomers of **AzoGW1929** (C) and **AzoRosi** (G) (25 μ M in DMSO) with alternating illumination at 320 nm and 420 nm). Photostationary states of **AzoGW1929** (D) in MeOD-d₄ and **AzoRosi** (H) in CDCl₃ of the dark-adapted state and after irradiation with 460 nm and 365 nm for five minutes.

The photophysical properties and photostationary states (PSS) of **AzoGW1929** and **AzoRosi** were determined by UV-Vis and ¹H-NMR spectroscopy (Figure 2). The absorption spectra after illumination with λ = 460 nm (*trans*, blue) and λ = 365 nm (*cis*, gray) demonstrated wavelength-dependent switching as expected for ‘classical’ unsubstituted azobenzenes. **AzoGW1929** showed an additional local absorption maximum at 400 nm which is likely caused by additional absorption

of the benzophenone moiety. Photoswitching was repeated over multiple cycles indicating good photostability of these photohormones. Photostationary states could further be titrated using different wavelengths of light ('color-dosing'). Half-life times of the thermally unstable *cis*-isomer were determined in DMSO at room temperature (Figure S1) and are $t_{1/2} = 37.0$ h (**AzoGW1929**) and $t_{1/2} = 64.1$ h (**AzoRosi**). The PSS after illumination with the optimal wavelengths for photoisomerization ($\lambda = 365$ nm and $\lambda = 460$ nm, respectively) are as follows: 95 % *trans*-**AzoGW1929** (dark), 76 % *trans*-**AzoGW1929** (460 nm), 67 % *trans*-**AzoGW1929** (365 nm) and 100 % *trans*-**AzoRosi** (dark), 80 % *trans*-**AzoRosi** (460 nm) and 4 % *trans*-**AzoRosi** (365 nm). These data revealed slow switching kinetics for **AzoGW1929**, whereas illumination with 365 nm allows for effective isomerization of **AzoRosi**.

The biological evaluation of the photohormones for modulation of PPAR γ was performed using hybrid Gal4 reporter gene assays in HEK293T cells. These test systems rely on chimeric transcription factors composed of the respective human nuclear receptor ligand binding domain and the DNA binding domain of the yeast protein Gal4. Gal4-responsive firefly luciferase was employed as reporter gene and a constitutively expressed *Renilla* luciferase served for normalization and to monitor test compound toxicity. Pioglitazone (1 μ M) served as reference agonist on every plate to calculate relative activation efficacy of the test compounds. To individually characterize both isomers of the photohormones, the assays were conducted with the *trans*-photohormones in the dark and with the pre-illuminated *cis*-isomers using a Cell Disco⁴³.

Profiling of the three first-generation photohormones **AzoMDG548**, **AzoGW1929** and **AzoRosi** revealed no activity for *trans*-**AzoMDG548** on PPAR γ up to 10 μ M concentration while *trans*-**AzoGW1929** and *trans*-**AzoRosi** were confirmed as PPAR γ modulators with promising potencies and activation efficacies (Table 1). Preliminary evaluation of the *cis*-counterparts revealed similar activity on PPAR γ as for the *trans*-isomers which aligned with our observations in the docking studies. Except for weak activity of **AzoRosi** on PPAR α at 10 μ M, all three photohormones were

selective for PPAR γ over the closely related PPAR α and PPAR δ subtypes. Due to the lack of activity of **AzoMDG548**, we did not further characterize this compound and focused our further study on the other two lead compounds.

Table 1. PPAR modulatory activity of photohormones **AzoMDG548**, **AzoGW1929** and **AzoRosi** in a Gal4 hybrid reporter gene assay. Maximum relative activation (max. rel. act.) refers to the activity of 1 μ M pioglitazone. Data are the mean \pm SD. Each sample was tested in technical duplicates in at least two independent biological repeats. Inactive - no statistically significant activity at 10 μ M.

ID	PPAR γ modulation	PPAR α modulation	PPAR δ modulation
<i>trans</i> - AzoMDG548	inactive	inactive	inactive
<i>trans</i> - AzoGW1929	EC ₅₀ = 1.0 \pm 0.1 μ M (30 \pm 2% max. rel. act.)	inactive	inactive
<i>trans</i> - AzoRosi	EC ₅₀ = 2.2 \pm 0.2 μ M (21 \pm 1% max. rel. act.)	8% activation at 10 μ M	inactive

Encouraged by the favorable PPAR γ modulatory activity and promising photophysical characteristics of **AzoGW1929** and **AzoRosi**, we selected both photohormones for further structural refinement. Analysis of the predicted binding mode of **AzoGW1929** in the PPAR γ ligand binding site indicated occupation of the sub-pocket accommodating the azobenzene motif with little space for further derivatization. However, we observed potential for a chlorine substituent in position 4 of the azobenzene moiety to generate preference for the *trans*-configuration since docking simulation of **AzoGW1929-2** in the GW1929-bound structure (PDB ID: 6D8X) revealed favorable binding for the *trans*-isomer but no reasonable pose for the *cis*-counterpart (Figure 3A). The docking pose of **AzoRosi** suggested an opportunity for structural refinement, too. As discussed above, the benzylthiazolidinedione motif has been characterized as essential for

activity, prompting us to focus on the azobenzene part for optimization. In the docked *trans*-configuration of **AzoRosi**, the azobenzene was bound in a cavity with little space available for substituents. However, **AzoRosi** analogs bearing bulky substituents in position 4 of the azobenzene motif were observed to bind favorably to PPAR γ in *cis*-configuration, with the extra substituents protruding into to an unoccupied pocket of the Y-shaped PPAR γ ligand binding site (Figure 3B). This optimization potential seemed particularly attractive as it suggested preference for the *cis*-configurations of **AzoRosi** descendants. The effect was observed in the molecular docking of **AzoRosi-2** bearing a chlorine atom in position 4 of the azobenzene motif, and even more pronounced for the trifluoromethyl analog **AzoRosi-3**. **AzoRosi-4** was designed as maximally *cis*-favoring structure according to our results in the molecular docking. The *cis*-isomer of **AzoRosi-4** formed a favorable binding mode to the PPAR γ ligand binding site (Figure 3B & 5A) with H-bond interactions to the canonical activation triad of PPAR γ (His323, His449, Tyr473). The extended and lipophilic biphenylazobenzene protruded to a hydrophobic tunnel in the Y-shaped PPAR γ pocket formed by Ile281 and the backbones of Gly284 and Cys285 from helix 3 as well as Ile341 and Met348 from the beta sheet near helix 6. In contrast, the extended linear structure of *trans*-**AzoRosi-4** could not be reasonably placed in the angled PPAR γ ligand binding site.

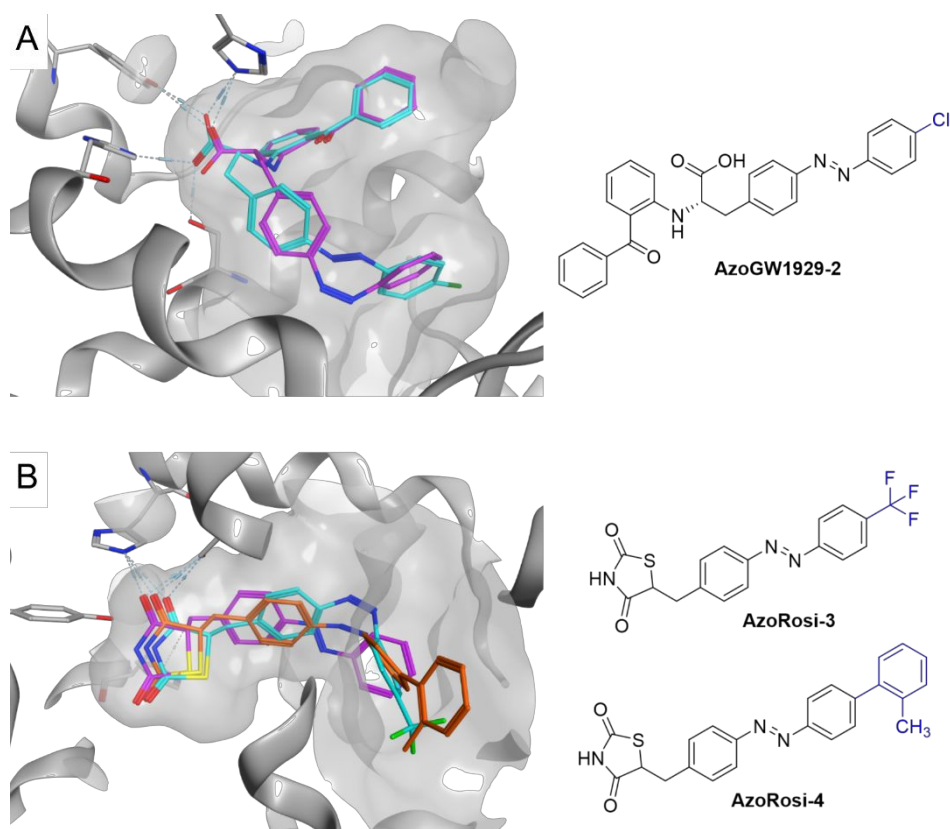


Figure 3. Molecular docking study to design optimized **AzoGW1929** (A, magenta) and **AzoRosi** (B, magenta) derivatives. Docking was performed in MOE using X-ray crystal structures of PPAR γ complexed with the template ligands GW1929 (A, PDB ID: 6D8X) and Rosiglitazone (B, PDB ID: 5YCP). (A) Docking simulations suggested that introduction of a chlorine substituent in position 4 of the azobenzene residue in **AzoGW1929-2** (cyan) would promote preferential binding of the *trans*-isomer. (B) *cis*-**AzoRosi-3** (cyan) and *cis*-**AzoRosi-4** (orange) favorably extended to a tunnel in the PPAR γ ligand binding site that is not occupied by the template ligand Rosiglitazone or by **AzoRosi**.

The second generation azologs **AzoGW1929-2** and **AzoRosi-2** to **AzoRosi-4** were prepared as described in Scheme 1. Their photophysical properties are depicted in Figure 4 and Figure S1. The spectra of **AzoGW1929-2** showed photophysical properties similar to the unsubstituted parent azolog **AzoGW1929**. Photophysical evaluation of **AzoRosi-2** to **AzoRosi-4** also showed that these analogs behaved similar to their predecessor **AzoRosi**, with respect to absorption spectra

for both isomers, switching kinetics, thermal stability of the *cis*-isomer and PSS (99 % *trans*-**AzoRosi-4** (dark), 83 % *trans*-**AzoRosi-4** (460 nm) and 23 % *trans*-**AzoRosi-4** (365 nm)).

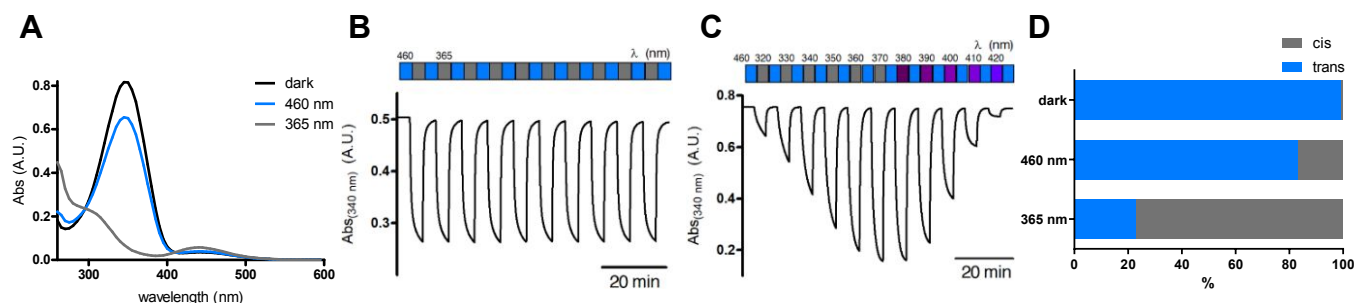
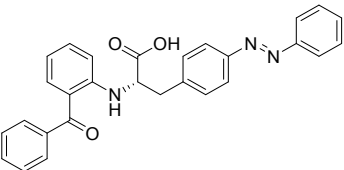
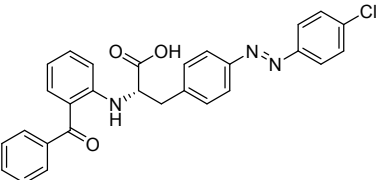
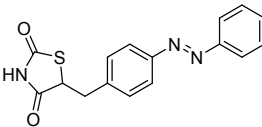
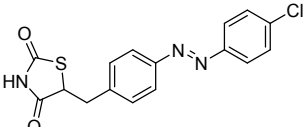
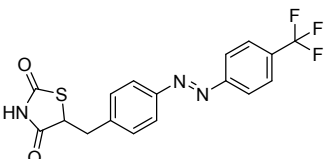
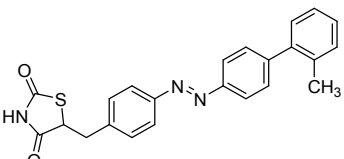


Figure 4. (A) Photophysical evaluation of **AzoRosi-4** (25 μ M in DMSO) in the dark-adapted (*trans*, black), 365 nm-adapted (*cis*, gray) and 460 nm-adapted (*trans*, blue) photostationary states. Reversible cycling of **AzoRosi-4** (25 μ M in DMSO) with alternating illumination at 365 nm and 460 nm (B) or with alternating illumination at wavelengths between 320 nm and 420 nm (C). (D) Photostationary States of **AzoRosi-4** in CDCl₃ of the dark-adapted state and after irradiation with 460 nm and 365 nm.

Biological evaluation of **AzoGW1929-2** for PPAR γ modulation revealed neither improved potency nor a clear preference for either isomer (Table 2). This chemotype, therefore, seems to hold little promise for continued refinement and was not further pursued. **AzoRosi-2**, which bears a chlorine substituent on the azobenzene, was almost equally active as *trans*-**AzoRosi** in its *trans*-configuration and showed enhanced PPAR γ activation in its *cis*-configuration (Table 2). This agrees with our hypothesis that extension of **AzoRosi** in position 4 of the azobenzene would promote preferential PPAR γ agonism of the *cis*-isomer. Accordingly, the *cis*-isomer of the trifluoromethyl derivative **AzoRosi-3** was more active than *trans*-**AzoRosi-3**. However, the maximum activation efficacy of dark-adapted *trans*-**AzoRosi-3** was also higher than that of its parent azolog *trans*-**AzoRosi**. By contrast, the *o*-toluyl derivative **AzoRosi-4** was less active in its *trans*-configuration than *trans*-**AzoRosi** (12% vs. 21% maximum activation), while the *cis*-isomer of **AzoRosi-4** increased its PPAR γ agonism approximately threefold with 39% maximum relative

activation efficacy (Table 2). Therefore, **AzoRosi-4** is a photohormone for PPAR γ that can be activated with light. This relative dark-inactivity and gain in potency upon irradiation is a desirable functional feature in photopharmacology.

Table 2. Light-dependent PPAR γ modulatory activity of photohormones **AzoGW1929**, **AzoGW1929-2**, **AzoRosi** and **AzoRosi-2-4** in a Gal4 hybrid reporter gene assay. Maximum relative activation (max. rel. act.) refers to the activity of 1 μ M Pioglitazone. Data are the mean \pm SD. Each sample was tested in technical duplicates in at least two independent biological repeats.

ID	structure	PPAR γ modulation	
		<i>trans</i>	<i>cis</i>
AzoGW1929		EC ₅₀ = 1.0 \pm 0.1 μ M (30 \pm 2% max. rel. act.)	EC ₅₀ = 1.30 \pm 0.01 μ M (27.2 \pm 0.1% max. rel. act.)
AzoGW1929-2		EC ₅₀ = 1.6 \pm 0.1 μ M (20 \pm 1% max. rel. act.)	EC ₅₀ = 5.0 \pm 0.4 μ M (35 \pm 2% max. rel. act.)
AzoRosi		EC ₅₀ = 2.2 \pm 0.2 μ M (21 \pm 1% max. rel. act.)	EC ₅₀ = 6.3 \pm 1.4 μ M (38 \pm 5% max. rel. act.)
AzoRosi-2		EC ₅₀ = 2.9 \pm 0.2 μ M (25 \pm 1% max. rel. act.)	EC ₅₀ = 7.0 \pm 1.0 μ M (49 \pm 4% max. rel. act.)
AzoRosi-3		EC ₅₀ = 2.2 \pm 0.7 μ M (33 \pm 5% max. rel. act.)	EC ₅₀ = 6.5 \pm 1.5 μ M (52 \pm 11% max. rel. act.)
AzoRosi-4		EC ₅₀ = 2.8 \pm 1.3 μ M (12 \pm 2% max. rel. act.)	EC ₅₀ = 6.4 \pm 0.4 μ M (39 \pm 2% max. rel. act.)

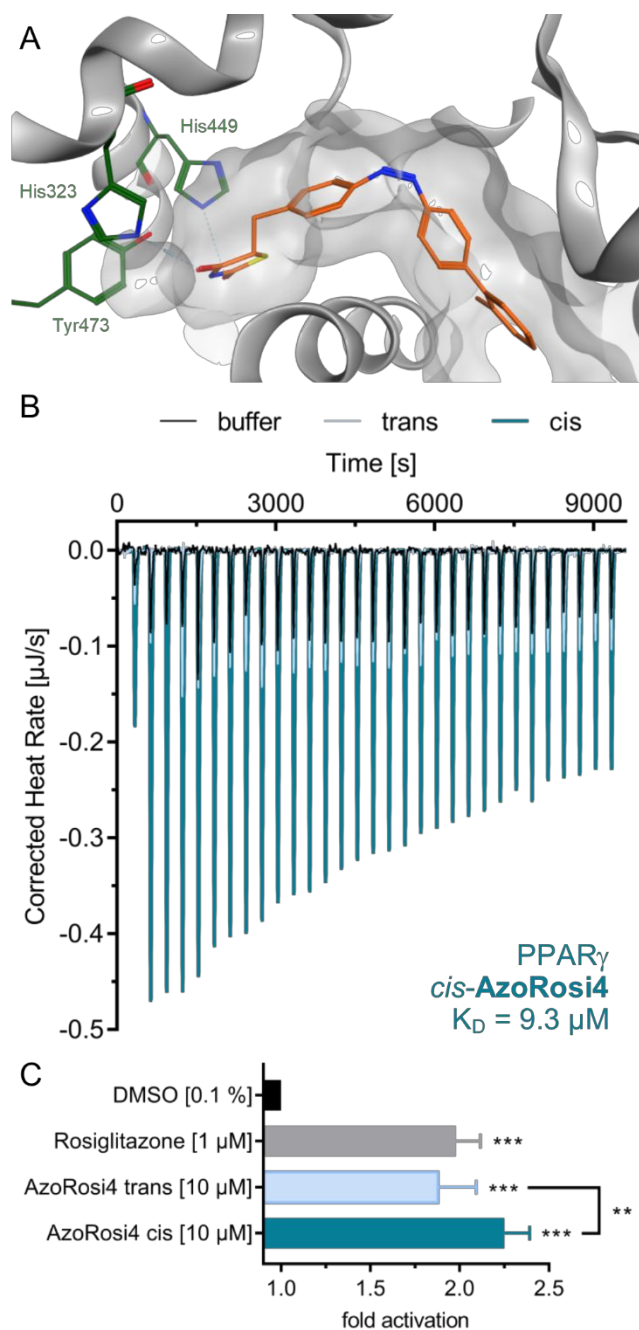


Figure 5. (A) Molecular docking of *cis*-AzoRosi4 to the PPAR γ ligand binding site (PDB ID: 5YCP). (B) Isothermal titration calorimetry experiment of *trans*-AzoRosi-4 (dark-adapted, 300 µM) and *cis*-AzoRosi-4 (irradiated with $\lambda=365$ nm for 5 minutes, 300 µM) to recombinant PPAR γ ligand binding domain protein revealed exclusive binding of *cis*-AzoRosi-4. Buffer as control. $K_D = 9.3$ µM. Colors are specified in the figure. Individual titrations are shown in Figure

S3 (Supporting Information). (C) *cis*-**AzoRosi-4** robustly activated the human PPAR response element (PPRE) in the absence of receptor overexpression in HepG2 cells. Rosiglitazone served as reference agonist for PPAR γ activation. Data are the mean \pm SD. Each sample was tested in technical duplicates in six independent biological repeats; ** $p < 0.01$, *** $p < 0.001$ (t-test).

Next we determined the binding affinity of **AzoRosi-4** for both photo-isomers by isothermal titration calorimetry (ITC, Figure 5B). The light-activated *cis*-isomer bound to the recombinant PPAR γ ligand binding domain with a K_D value of 9.3 μ M. Under identical conditions, no binding of dark-adapted *trans*-**AzoRosi-4** was detectable in ITC, corroborating the predicted binding of *cis*-**AzoRosi-4** (Figure 5A) and the anticipated clashes of the *trans*-isomer with the PPAR γ ligand binding site.

Next we probed *cis*-**AzoRosi-4** for the ability to activate endogenous PPAR γ in cellular setting. Given the complex regulation of transcriptional control by various transcription factors and potential compensatory effects on expression levels of PPAR γ target genes, we aimed to analyze target engagement in native liver cells with a reliable luminescent readout. For this, we transiently transfected PPAR γ expressing HepG2 cells with a reporter construct comprising the human full-length PPAR response element (PPRE) to control the expression of a firefly luciferase reporter gene. PPAR γ and its heterodimer partner RXR were not overexpressed to enable observation of endogenous cellular PPAR γ activation. The light-activated photohormone *cis*-**AzoRosi-4** activated the PPRE reporter with an EC_{50} value of 0.9 ± 0.2 μ M and 2.4 ± 0.1 -fold maximum activation efficacy. Interestingly, despite the absence of binding affinity for *trans*-**AzoRosi-4** in the ITC some PPRE activation was observed in the cellular setting by the *trans*-isomer at 10 μ M (Figure 5C).

Conclusion and Outlook

In conclusion, we report on the computer-aided development of photohormones for the nuclear hormone receptor PPAR γ . Supported by docking simulations, we identified PPAR γ ligand chemotypes that allow for azologization and confirmed PPAR γ modulation for two out of three basic photohormones. Subsequent structure-guided optimization resulted in second generation photoswitchable analogs of Rosiglitazone that exhibit stronger PPAR γ activation in their *cis*-configuration. Among the seven PPAR γ -modulating photohormones developed in this study, **AzoRosi-4** was designed to have low biological activity in its native *trans*-configuration, but markedly activated PPAR γ upon light-activation to the *cis*-isomer. This successful computer-aided development of **AzoRosi-4** demonstrates that structure-guided design of azologs is feasible for proteins with highly flexible binding regions, such as PPAR γ . With its attractive activity profile and its favorable photophysical characteristics, **AzoRosi-4** emerges as first-in-class photohormone for PPAR γ enabling new types of *in vitro* studies with light-dosing of PPAR γ activation. This photohormone could become a useful tool for the study of PPAR γ biology, including spatiotemporal aspects of its regulation that cannot be studied with constitutively active modulators or caged compounds. These properties are particularly useful in the context of drug discovery, as adverse effect profiles have recently limited clinical use or development of PPAR γ agonists. A photohormone may, for example, be light-activated in certain tissues to activate PPAR γ for beneficial effects while other organs where the nuclear receptor mediates adverse activities – such as in the brain⁴⁴ or bone⁴⁵ – can be spared. Photohormones that can be locally activated at their desired site of action, potentially exhibit an improved pharmacological profile and could ultimately pave the road for novel drugs for the treatment of metabolic disorders (including diabetes mellitus and obesity). Our study underscores that photopharmacology is a promising approach for the precision control of nuclear hormone receptors, as we expanded the scope of photohormones to PPAR γ . Photohormones will allow the study of NHR biology with

unprecedented resolution in space and time and could potentially be useful for new forms of photodynamic therapy.^{46,47}

Experimental Section

General Information

All reagents and solvents were purchased from commercial sources (Sigma-Aldrich, TCI America, Strem Chemicals, Thermo Fischer Scientific, etc.) and were used without further purification. Reactions were monitored by TLC on pre-coated, Merck Silica gel 60 F₂₅₄ glass backed plates and the chromatograms were visualized by UV irradiation at $\lambda = 254$ nm. Flash silica gel chromatography was performed using silica gel (SiO₂, particle size 40-63 μ m) purchased from SiliCycle. NMR spectra were measured on a BRUKER Avance III HD 400 (equipped with CryoProbe™). Multiplicities in the following experimental procedures are abbreviated as follows: s = singlet, d = doublet, t = triplet, q = quartet, m = multiplet. Proton chemical shifts are expressed in parts per million (ppm, δ scale) and are referenced to the residual protium in the NMR solvent (CDCl₃: $\delta = 7.26$; DMSO-d₆: $\delta = 2.50$; MeOD-d₄: $\delta = 3.31$). Carbon chemical shifts are expressed in ppm (δ scale) and are referenced to the carbon resonance of the NMR solvent (CDCl₃: $\delta = 77.2$; DMSO-d₆: $\delta = 39.5$; MeOD-d₄: $\delta = 49.0$). *NOTE*: Due to the *trans/cis* isomerization of compounds containing an azobenzene functionality, more signals were observed in the ¹H-NMR and ¹³C-NMR spectra than expected for the pure *trans*-isomer. Only signals for the major *trans*-isomer are reported.

The purity of the compounds was measured on an Agilent Technologies 1260 II Infinity connected to an Agilent Technologies 6120 Quadrupole mass spectrometer with ESI ionization source. Elution was performed using a gradient from 25:75% to 100:0% MeCN:H₂O with 0.1% formic acid over 5 min and the whole UV-vis spectrum was recorded. The purity of all final compounds was $\geq 90\%$ for **AzoGW1929** and **AzoGW1929-2**, and $\geq 95\%$ for **AzoRosi**, **AzoRosi-2**, **AzoRosi-3** and

AzoRosi-4 as determined by high-performance liquid chromatography/UV-vis (HPLC-UV/Vis). UV-Vis spectra were recorded using a Varian Cary 50 Bio UV-Visible Spectrophotometer with BRAND Ultra-Micro UV-Cuvettes (10 mm light path). Further absorption measurements were performed on a FLUOstar Omega plate reader (BMG Labtech). The LED light sources were obtained from Amazon ($\lambda = 365$ nm and $\lambda = 460$ nm, P = 1.5 W) and LEDSupply (LuxStrip II LED bar, $\lambda = 660$ nm) respectively. Illumination for the reversible *trans* \leftrightarrow *cis* and action spectra was provided by an OptoSource Illuminator (CAIRN-Research) supplied by an OptoScan Power Supply (CAIRN-Research) and connected to an OptoScan Monochromator (CAIRN-Research). The Cell Disco System is in-house made⁴³.

Hybrid Reporter Gene Assays for PPAR α , PPAR γ and PPAR δ : The Gal4-fusion receptor plasmids pFA-CMV-hPPAR α -LBD, pFA-CMV-hPPAR γ -LBD and pFA-CMV-hPPAR δ -LBD coding for the hinge region and ligand binding domain of the canonical isoform of the respective nuclear receptor have been reported previously.⁴⁸ pFR-Luc (Stratagene) was used as the reporter plasmid and pRL-SV40 (Promega) for normalization of transfection efficiency and cell growth. HEK293T cells were obtained from DSMZ (German Collection of Microorganisms and Cell Culture GmbH) and tested for mycoplasma contamination.

PPRE reporter gene assay in PPAR γ expressing HepG2 cells: The reporter plasmid PPRE1-pGL3 coding for firefly luciferase reporter gene under control of the human full length PPAR response element (PPRE) has been described previously.⁴⁹ pRL-SV40 (Promega) was used for normalization of transfection efficiency and cell growth. HepG2 cells were obtained from DSMZ (German Collection of Microorganisms and Cell Culture GmbH) and tested for mycoplasma contamination.

(E)-5-(4-(phenyldiazenyl)benzylidene)-2-thioxodihydropyrimidine-4,6(1H,5H)-dione
(AzoMDG548)

Thiobarbituric acid (10.3 mg, 71.0 μmol , 1.00 eq.) was suspended in anhydrous EtOH (1.5 mL) and 4-phenylazo benzaldehyde **1** (15.0 mg, 71.0 μmol , 1.00 eq.) in EtOH (1 mL) was slowly added. After stirring at 80 °C for 2 h, the resulting solid was filtered off, washed with EtOH and dried under vacuum. The product was obtained as a dark-red solid (11.0 mg, 32.7 μmol , 46 %). ^1H NMR (400 MHz, DMSO- d_6) δ 12.51 (s, 1H), 12.40 (s, 1H), 8.35 (s, 1H), 8.30 (s, 1H), 8.28 (s, 1H), 7.95 – 7.93 (m, 4H), 7.64 – 7.62 (m, 3H). ^{13}C NMR (101 MHz, DMSO- d_6) δ 178.6, 161.5, 159.4, 153.7, 153.3, 152.0, 135.5, 134.4 (2C), 132.2, 129.6 (2C), 122.9 (2C), 121.9 (2C), 120.3. HRMS: m/z calc. for $\text{C}_{17}\text{H}_{13}\text{N}_4\text{O}_2\text{S}^+$ ($[\text{M}+\text{H}]^+$): 337.0754, found: 337.0755.

Methyl (S)-2-amino-3-(4-aminophenyl)propanoate 3

An oven-dried round bottom flask was charged with methyl (S)-2-amino-3-(4-nitrophenyl)propanoate **2** (1.00 g, 3.84 mmol, 1.00 eq.). The reaction vessel was evacuated and purged with nitrogen three times. Palladium on charcoal (81.7 mg, 76.8 μmol , 0.20 eq.) was added and the headspace was thoroughly purged with nitrogen before degassed MeOH (25 mL) was added. The nitrogen atmosphere was replaced by hydrogen and the suspension was saturated with hydrogen by sparging. The reaction mixture was stirred at room temperature for 16 h. The headspace was purged with nitrogen and the reaction mixture was filtered through a pad of silica with CH_2Cl_2 . The filtrate was concentrated, yielding the product as an off-white solid (751 mg, 3.97 mmol, quant.). ^1H NMR (400 MHz, MeOD- d_4) δ 6.98 (d, J = 8.5 Hz, 2H), 6.72 (d, J = 8.5 Hz, 2H), 4.21 (dd, J = 7.4, 5.8 Hz, 1H), 3.81 (s, 3H), 3.16 – 3.00 (m, 2H). ^{13}C NMR (101 MHz, MeOD- d_4) δ 170.7, 148.5, 131.1 (2C), 124.0, 117.0 (2C), 55.5, 53.5, 36.8. HRMS: m/z calc. for $\text{C}_{10}\text{H}_{15}\text{N}_2\text{O}_2^+$ ($[\text{M}+\text{H}]^+$): 195.1128, found: 195.1130.

Methyl (S,E)-2-amino-3-(4-(phenyldiazenyl)phenyl)propanoate 4 and

Methyl (S,E)-2-amino-3-(4-((4-chlorophenyl)diazenyl)phenyl)propanoate 5

Aniline/4-Chloroaniline (288 mg/394 mg, 3.10 mmol, 3.00 eq.) was dissolved in CH_2Cl_2 (15 mL) and Oxone (3.80 g, 6.12 mmol, 6.00 eq.) in water (15 mL) was added to the solution. The

suspension was vigorously stirred at room temperature for 16 h during which the reaction mixture turned green. The two phases were separated, and the organic phase was washed with 1M HCl, sat. aq. NaHCO₃, and water. The organic phase was dried over Na₂SO₄ before methyl (*S*)-2-amino-3-(4-aminophenyl)propanoate **3** (200 mg, 1.03 mmol, 1.00 eq.) and glacial acetic acid (2 mL) were added. The solution was concentrated under reduced pressure to remove CH₂Cl₂ and finally stirred at room temperature overnight. Acetic acid was removed by azeotropic distillation with toluene (three times). Flash column chromatography with CH₂Cl₂/MeOH (1:0 to 9:1) yielded the corresponding product as a yellow oil. **4** (203 mg, 71.7 μmol, 70 %): ¹H NMR (400 MHz, MeOD-d₄) δ 7.89 (t, *J* = 7.3 Hz, 4H), 7.54 (q, *J* = 9.2, 7.8 Hz, 3H), 7.41 (d, *J* = 8.3 Hz, 2H), 3.96 (t, *J* = 6.7 Hz, 1H), 3.73 (s, 3H), 3.18 (dd, *J* = 13.7, 6.3 Hz, 1H), 3.09 (dd, *J* = 13.7, 7.1 Hz, 1H). ¹³C NMR (101 MHz, MeOD-d₄) δ 174.6, 154.0, 153.1, 141.2, 132.3, 131.3 (2C), 130.3 (2C), 124.1 (2C), 123.8 (2C), 56.2, 52.8, 40.4. HRMS: *m/z* calc. for C₁₆H₁₈N₃O₂⁺ ([M+H]⁺): 284.1394, found: 284.1388. **5** (110 mg, 34.7 μmol, 34 %): ¹H NMR (400 MHz, MeOD-d₄) δ 7.88 (dd, *J* = 11.9, 8.6 Hz, 4H), 7.56 (d, *J* = 8.7 Hz, 2H), 7.40 (d, *J* = 8.3 Hz, 2H), 3.79 (t, *J* = 6.7 Hz, 1H), 3.69 (s, 3H), 3.15 – 2.99 (m, 2H). ¹³C NMR (101 MHz, MeOD-d₄) δ 176.1, 152.8, 152.5, 142.6, 138.0, 131.3 (2C), 130.5 (2C), 125.2 (2C), 124.1 (2C), 56.6, 52.4, 41.6. HRMS: *m/z* calc. for C₁₆H₁₇ClN₃O₂⁺ ([M+H]⁺): 318.1004, found: 318.0991.

(*S,E*)-2-((2-benzoylphenyl)amino)-3-(4-(phenyldiazenyl)phenyl)propanoic acid

(AzoGW1929) and (*S,E*)-2-((2-benzoylphenyl)amino)-3-(4-((4-chlorophenyl)diazenyl)-phenyl)propanoic acid (AzoGW1929-2)

An oven-dried microwave vessel was charged with methyl (*S,E*)-2-amino-3-(4-(phenyldiazenyl)phenyl)propanoate **4** / methyl (*S,E*)-2-amino-3-(4-((4-chlorophenyl)diazenyl)-phenyl)propanoate **5** (50.0 mg, 176.4 μmol/157.4 μmol, 1.20 eq.), (2-bromophenyl)(phenyl)methanone (34.3 mg, 132.2 μmol, 1.00 eq.), Cs₂CO₃ (111 mg, 341 μmol, 2.60 eq.), Pd(OAc)₂ (2.9 mg, 13 μmol, 10 mol %) and (+/-)-BINAP (12.3 mg, 19.7 μmol, 0.15 eq.) in toluene (2 mL). The reaction mixture was stirred at 110 °C for 3 h under a nitrogen atmosphere.

Subsequently, the reaction was quenched with water, diluted with EtOAc and filtered through a pad of silica. The filtrate was concentrated and the residue was purified by flash column chromatography (hexanes/EtOAc 1/0 to 1/1) to give the product as a viscous orange oil. Methyl (*S,E*)-2-((2-benzoylphenyl)amino)-3-(4-(phenyldiazenyl)phenyl)propanoate / Methyl (*S,E*)-2-((2-benzoylphenyl)amino)-3-(4-((4-chlorophenyl)diazenyl)phenyl)propanoate (39.2 mg/21.7 mg, 84.6 μ mol/43.6 μ mol, 1.00 eq.) was dissolved in acetonitrile (0.5 mL) and an aqueous solution of LiOH (5.1 mg/2.6 mg, 0.21 mmol/0.11 mmol, 2.5 eq. in 0.5 mL H₂O) was added. The mixture was stirred at 0 °C for 30 minutes and then acidified to pH=2 with 1 M HCl. The aqueous phase was extracted with CH₂Cl₂ three times and the combined organic layers were dried over Na₂SO₄ and concentrated to give the desired product as a red solid. **AzoGW1929** (37.0 mg, 82.3 μ mol, 97 %): ¹H NMR (400 MHz, CDCl₃) δ 7.87 (ddd, *J* = 10.7, 7.6, 1.7 Hz, 4H), 7.60 (dt, *J* = 6.9, 1.4 Hz, 2H), 7.53 – 7.43 (m, 9H), 7.39 (t, *J* = 7.8 Hz, 1H), 6.73 – 6.63 (m, 2H), 4.48 (dd, *J* = 7.8, 5.3 Hz, 1H), 3.45 (dd, *J* = 13.9, 5.2 Hz, 1H), 3.29 (dd, *J* = 13.8, 8.0 Hz, 1H). ¹³C NMR (101 MHz, CDCl₃) δ 199.6, 174.5, 152.8, 151.9, 149.9, 140.1, 139.4, 135.7, 135.2, 131.3, 131.1, 130.3, 129.4 (2C), 129.3, 129.2 (2C), 128.3, 123.4 (2C), 123.0 (2C), 119.0, 116.1, 112.3, 57.9, 38.6, 29.9. HRMS: *m/z* calc. for C₂₈H₂₃N₃NaO₃⁺ ([M+Na]⁺): 472.1632, found: 472.1652. **AzoGW1929-2** (19.5 mg, 40.3 μ mol, 93 %): ¹H NMR (400 MHz, CDCl₃) δ 8.88 (s, 1H), 7.84 (dd, *J* = 8.5, 2.8 Hz, 4H), 7.61 – 7.57 (m, 2H), 7.53 – 7.42 (m, 8H), 7.39 (t, *J* = 7.8 Hz, 1H), 6.70 (d, *J* = 8.5 Hz, 1H), 6.66 (t, *J* = 7.5 Hz, 1H), 4.49 (dd, *J* = 7.9, 5.2 Hz, 1H), 3.44 (dd, *J* = 13.9, 5.1 Hz, 1H), 3.28 (dd, *J* = 13.9, 7.8 Hz, 1H). ¹³C NMR (101 MHz, CDCl₃) δ 199.6, 174.3, 151.7, 151.1, 149.9, 140.1, 139.8, 137.0, 135.7, 135.2, 131.3, 130.3, 129.5 (2C), 129.3 (2C), 128.3, 124.2 (2C), 123.4 (2C), 119.0, 116.1, 112.3, 57.8, 38.6, 29.9, 14.3. HRMS: *m/z* calc. for C₂₈H₂₂ClN₃NaO₃⁺ ([M+Na]⁺): 506.1242, found: 506.1257.

(E)-5-(4-(phenyldiazenyl)benzyl)thiazolidine-2,4-dione (AzoRosi) and

(E)-5-(4-((4-chlorophenyl)diazenyl)benzyl)thiazolidine-2,4-dione (AzoRosi-2) and

(E)-5-(4-((4-(trifluoromethyl)phenyl)diazenyl)benzyl)thiazolidine-2,4-dione (AzoRosi-3) and

(E)-5-(4-((2'-methyl-[1,1'-biphenyl]-4-yl)diazenyl)benzyl)thiazolidine-2,4-dione (AzoRosi-4)

Aniline/4-Chloroaniline/4-(trifluoromethyl)aniline/2'-methyl-[1,1'-biphenyl]-4-amine (31.4 mg/43.0 mg/54.4 mg/61.8 mg, 337 μmol , 3.00 eq.) was dissolved in CH_2Cl_2 (2 mL) and Oxone (415 mg, 675 μmol , 6.00 eq.) in water (2 mL) was added to the solution. The suspension was vigorously stirred at room temperature for 16 h, during which the mixture turned green. The two phases were separated, and the organic phase was washed with 1 M HCl, sat. aq. NaHCO_3 , and water. The organic phase was dried over Na_2SO_4 before 5-(4-aminobenzyl)thiazolidine-2,4-dione **7** (25.0 mg, 113 μmol , 1.00 eq.), was synthesized according to literature procedures⁴¹) and glacial acetic (250 μL) acid was added. The solution was concentrated under reduced pressure to remove the CH_2Cl_2 and finally stirred at room temperature overnight. The acetic acid was removed by azeotropic distillation with toluene (three times) and removed under reduced pressure three times. Flash column chromatography with $\text{CH}_2\text{Cl}_2/\text{MeOH}$ (1:0 to 9:1) yielded the corresponding product as a yellow solid. **AzoRosi** (25.2 mg, 80.9 μmol , 72 %): ^1H NMR (400 MHz, CDCl_3) δ 7.90 (t, J = 8.0 Hz, 4H), 7.52 (q, J = 10.1, 9.2 Hz, 3H), 7.40 (d, J = 8.2 Hz, 2H), 4.60 (dd, J = 9.5, 4.0 Hz, 1H), 3.61 (dd, J = 14.1, 3.9 Hz, 1H), 3.26 (dd, J = 14.1, 9.5 Hz, 1H). ^{13}C NMR (101 MHz, CDCl_3) δ 173.9, 170.0, 152.7, 152.2, 138.8, 131.3, 130.2 (2C), 129.3 (2C), 123.4 (2C), 123.0 (2C), 53.1, 38.5. HRMS: m/z calc. for $([\text{M}+\text{H}]^+)$: 312.0801, found: 312.0788. **AzoRosi-2** (27.7 mg, 80.1 μmol , 71 %): ^1H NMR (400 MHz, CDCl_3) δ 7.87 (dd, J = 8.3, 6.0 Hz, 4H), 7.49 (d, J = 8.7 Hz, 2H), 7.39 (d, J = 8.3 Hz, 2H), 4.59 (dd, J = 9.4, 4.0 Hz, 1H), 3.60 (dd, J = 14.1, 3.9 Hz, 1H), 3.26 (dd, J = 14.1, 9.5 Hz, 1H). ^{13}C NMR (101 MHz, CDCl_3) δ 173.5, 169.6, 152.1, 151.1, 139.1, 137.3, 130.3 (2C), 129.5 (2C), 124.3 (2C), 123.5 (2C), 53.0, 38.5. HRMS: m/z calc. for $([\text{M}+\text{H}]^+)$: 346.0412, found: 346.0401. **AzoRosi-3** (24.3 mg, 64.1 μmol , 57 %): ^1H NMR (400 MHz, CDCl_3) δ 7.99 (d, J = 8.3 Hz, 2H), 7.92 (d, J = 8.0 Hz, 2H), 7.78 (d, J = 8.3 Hz, 2H), 7.41 (d, J = 8.1 Hz, 2H), 4.60 (dd, J = 9.4, 3.8 Hz, 1H), 3.61 (dd, J = 14.1, 4.0 Hz, 1H), 3.28 (dd, J = 14.1, 9.4 Hz, 1H). ^{13}C NMR (101 MHz, CDCl_3) δ 173.7, 169.8, 154.5, 152.0, 139.7, 132.5 (q, J = 32.5 Hz, 2C), 130.3 (2C), 126.5 (q, J = 3.8 Hz, 2C), 124.0 (q, J = 272.4 Hz, 2C), 123.8, 123.2, 53.0, 38.5. ^{19}F NMR (377 MHz,

CDCl₃) δ 0.29, 0.17. HRMS: m/z calc. for ([M+H]⁺): 360.0675, found: 380.0662. **AzoRosi-4** (21.9 mg, 54.5 μ mol, 49 %): ¹H NMR (400 MHz, CDCl₃) δ 7.97 (d, J = 8.3 Hz, 2H), 7.91 (d, J = 8.2 Hz, 2H), 7.49 (d, J = 8.2 Hz, 2H), 7.41 (d, J = 8.2 Hz, 2H), 7.30 (m, 4H), 4.60 (dd, J = 9.5, 3.9 Hz, 1H), 3.62 (dd, J = 14.1, 3.8 Hz, 1H), 3.26 (dd, J = 14.0, 9.6 Hz, 1H), 2.32 (s, 3H). ¹³C NMR (101 MHz, CDCl₃) δ 173.7, 169.8, 152.3, 151.5, 145.2, 141.1, 138.7, 135.5, 130.7 (2C), 130.2 (2C), 129.8 (2C), 127.9, 126.1, 123.5 (2C), 122.8 (2C), 53.1, 38.6, 20.6. HRMS: m/z calc. for ([M+H]⁺): 402.1271, found: 402.1261.

2'-methyl-[1,1'-biphenyl]-4-amine **9**

An oven-dried miniature reflux equipment was charged with (4-aminophenyl)boronic acid **8** (192 mg, 1.40 mmol, 1.20 eq.), 2-bromotoluene (200 mg, 1.18 mmol, 1.00 eq.) and Pd(PPh₃)₄ (67.6 mg, 58.5 μ mol, 5 mol %) in DMF (5 mL). Potassium carbonate (1.10 g, 7.96 mmol, 6.74 eq.) in H₂O (6 mL) was added and the mixture was heated to 85 °C and stirred for 16 h under a nitrogen atmosphere. The reaction mixture was cooled to room temperature and extracted with CH₂Cl₂ three times. The combined organic layers were dried over Na₂SO₄, concentrated under reduced pressure and purified by flash column chromatography (hexanes/EtOAc 1/0 to 1/3), yielding the product as a yellow viscous oil (118 mg, 641 μ mol, 55 %). ¹H NMR (400 MHz, CDCl₃) δ 7.24-7.21 (m, 4H), 7.14 (d, J = 8.4 Hz, 2H), 6.77 (d, J = 8.3 Hz, 2H), 4.09 (s, 2H), 2.29 (s, 3H). ¹³C NMR (101 MHz, CDCl₃) δ 145.3, 142.1, 135.6, 132.4, 130.4, 130.3 (2C), 130.0, 126.8, 125.9, 114.9 (2C), 20.7. HRMS: m/z calc. for C₁₃H₁₄N⁺ ([M+H]⁺): 184.1121, found: 184.1118.

Crystallography

The X-ray intensity data of Thiazolidinedione **6** were measured on an Oxford Diffraction Xcalibur 3 system equipped with a graphite monochromator and a sealed-tube Mo K α X-ray tube (λ = 0.71073 Å). The frames were integrated with the Agilent CrysAlis PRO software package⁵⁰. Data were corrected for absorption effects using the Multi-Scan method (ABSPACK embedded in the Agilent CrysAlis PRO software package). The structure was solved with SIR97⁵¹ and refined with

SHELXL⁵². All C-bound hydrogen atoms have been calculated in ideal geometry riding on their parent atoms while the N-bound hydrogen atoms has been refined freely. The figures have been drawn at the 50% ellipsoid probability level⁵³. Crystallographic data for Thiazolidinedione **6** are available free of charge from the Cambridge Crystallographic Data Centre via http://www.ccdc.cam.ac.uk/data_request/cif (accession ref. CCDC 1997329). The X-ray intensity data of **AzoRosi-3** were measured on a Bruker D8 Venture TXS system equipped with a multilayer mirror monochromator and a Mo K α rotating anode X-ray tube (λ = 0.71073 Å). The frames were integrated with the Bruker SAINT software package⁵⁴. Data were corrected for absorption effects using the Multi-Scan method (SADABS)⁵⁵. The structure was solved with SIR97 and refined with SHELXL. All hydrogen atoms have been calculated in ideal geometry riding on their parent atoms. The figures have been drawn at the 50% ellipsoid probability level. There are two formula units in the asymmetric unit. Crystallographic data for **AzoRosi-3** are available free of charge from the Cambridge Crystallographic Data Centre via http://www.ccdc.cam.ac.uk/data_request/cif (accession ref. CCDC 1997328).

Computational Methods

General: Calculations were performed in Molecular Operating Environment (MOE, version 2018.0101, Chemical Computing Group Inc. Montreal, QC, Canada) using default settings for each tool/function unless stated otherwise. Amber10:EHT was used as default force field for all calculations. Molecular Docking: Docking was performed using X-ray structures of the PPAR γ ligand binding domain (LBD) complexed with different ligands, each serving for a different photohormone series based on structural similarity of the bound ligand and the photohormone. For GW1929 azologs, docking was performed using the X-ray structure of the PPAR γ LBD in complex with the parent compound GW1929 (PDB ID: 6D8X). For azologs of Rosiglitazone and MDG548, structure of the PPAR γ LBD in complex with Rosiglitazone was used for molecular docking (PDB ID: 5YCP). Protonation states of the complexes were adjusted using the MOE

QuickPrep tool. Redocking of the crystallized ligands resulted in binding poses with RMSD 0.5994 relative to the crystallized binding mode for GW1929 and RMSD 0.1871 for Rosiglitazone, respectively. The compounds were prepared using the MOE Wash tool: Protonation state dominant at pH 7; Coordinates Rebuild 3D; Preserved Existing Chirality. Docking was performed using the following settings in the MOE Dock tool: Receptor: Receptor + Solvent; Site: Ligand Atoms; Placement: Triangle Matcher; Score: London dG; Poses: 100; Refinement: Rigid receptor; Refinement Score: GBVI/WSA dG; Poses: 10. The highest ranked binding-mode with the carboxylate or thiazolidinedione participating in the H-bond network with the canonical activation triad was used. The respective co-crystallized template ligands GW1929 and Rosiglitazone and the parent compound MDG548 are colored in green, the respective azologs **AzoMDG548**, **AzoGW1929** and **AzoRosi** are colored in magenta. The second generation azologs **AzoGW1929-2** and **AzoRosi-3** are colored cyan, whereas **AzoRosi-4** is colored orange.

Photophysical Characterization and Photostationary States (PSS)

UV-Vis spectra were recorded using a Varian Cary 50 Bio UV-Visible Spectrophotometer with BRAND Ultra-Micro UV-Cuvettes (10 mm light path). Switching was achieved using $\lambda = 365$ nm or $\lambda = 460$ nm LED light sources. The LEDs were pointed directly into the top of the sample cuvette. An initial spectrum of all photohormones (25 μ M in DMSO) was recorded (dark-adapted state, black) and then again following illumination at $\lambda = 365$ nm for two minutes (*cis*-adapted state, gray). A third spectrum was recorded after irradiation at $\lambda = 460$ nm for two minutes (*trans*-adapted state, blue). In order to obtain the reversible *trans* \leftrightarrow *cis* spectrum, absorption at $\lambda_{\text{Abs}} = 340$ nm was constantly measured while alternating illumination at $\lambda = 365$ nm or $\lambda = 460$ nm for the indicated times allowed for rapid isomerization of the photohormones (25 μ M in DMSO). Therefore, a mercury lamp with a power of 75 watts connected to a monochromator was directly pointed into the top of the sample cuvette, providing irradiation via an optic fiber cable with the two distinct wavelengths $\lambda = 365$ nm and 460 nm for four minutes each (absorption was read at

$\lambda_{\text{Abs}} = 340 \text{ nm}$). For the color-dosing experiment, the same experimental setup comprising the mercury lamp, monochromator and optic fiber cable were used. The monochromator allowed for illumination of the photohormones (25 μM in DMSO) with the indicated wavelengths for four minutes each ($\lambda_{\text{Abs}} = 340 \text{ nm}$). Determination of the half-life was achieved by illumination of the photohormones (25 μM in DMSO) with $\lambda = 365 \text{ nm}$ for five minutes to yield the corresponding *cis*-isomers. Then, the sample has been excluded from light and absorption was read at room temperature every minute for 2 days. Fitting of the experimental data provided for the half-life time, assuming a one-phase decay. The photostationary states were determined by ^1H -NMR. Therefore, 1 mg of the corresponding photohormone was dissolved in deuterated solvent (CDCl_3 or MeOD-d_4) and a ^1H spectrum was recorded before (dark-adapted) and after illumination with $\lambda = 365 \text{ nm}$ (*cis*-adapted) and $\lambda = 460 \text{ nm}$ (*trans*-adapted) for five minutes. Integration of characteristic product peaks and normalization yielded the PSS.

In Vitro Pharmacological Characterization

Hybrid Reporter Gene Assay

HEK293T cells were cultured in Dulbecco's modified Eagle's medium (DMEM), high glucose with 10 % fetal calf serum (FCS), sodium pyruvate (1 mM), penicillin (100 U/mL), and streptomycin (100 $\mu\text{g/mL}$) at 37 $^\circ\text{C}$ and 5 % CO_2 . Twenty-four hours before transfection, cells were seeded in 96-well plates (3×10^4 cells/well). Before transfection, medium was changed to Opti-MEM without supplements. Transient transfection was carried out using Lipofectamine LTX reagent (Invitrogen) according to the manufacturer's protocol with pFR-Luc (Stratagene), pRL-SV40 (Promega), and the corresponding Gal4-fusion nuclear receptor plasmid. Five hours after transfection, medium was changed to Opti-MEM supplemented with penicillin (100 U/mL), streptomycin (100 $\mu\text{g/mL}$), and additionally containing 0.1 % dimethyl sulfoxide (DMSO) and the respective test compound or 0.1 % DMSO alone as untreated control. Each concentration was tested in duplicates and each experiment was repeated independently at least two times. After overnight (14–16 h) incubation

the cells were assayed for luciferase activity using the Dual-Glo Luciferase Assay System (Promega) according to the manufacturer's protocol. Luminescence was measured with a Tecan Spark luminometer (Tecan Deutschland GmbH, Germany). Normalization of transfection efficiency and cell growth was done by division of firefly luciferase data by *Renilla* luciferase data and multiplying the value by 1000 resulting in relative light units (RLU). Fold activation was obtained by dividing the mean RLU of test compound by the mean RLU of the untreated control. Max. relative activation refers to fold reporter activity divided by the fold activation of respective reference agonist (at a concentration of 1 μ M) treated cells. All hybrid assays were validated with the respective reference agonists (PPAR α : GW7647; PPAR γ : pioglitazone; PPAR δ : L165041) which yielded EC₅₀ values in agreement with the literature. Characterization of the respective *cis*-counterparts was performed in the same way with pre-irradiated compounds (irradiation for 3 min at λ = 365 nm right before incubation). To maintain the compound in *cis*-adapted state, the Cell Disco System was used during incubation with 75 ms light pulses (λ = 370 nm) every 15 s.

PPRE Reporter Assay in HepG2

HepG2 cells were cultured in Dulbecco's modified Eagle's medium (DMEM), high glucose with 10% fetal calf serum (FCS), sodium pyruvate (1 mM), penicillin (100 U/mL), and streptomycin (100 μ g/mL) at 37 °C and 5 % CO₂. Twenty-four hours before transfection, cells were seeded in 96-well plates (1.25×10^4 cells/well) pre-coated with Collagen G solution. Before transfection, medium was changed to Opti-MEM without supplements. Transient transfection was carried out using Lipofectamine 3000 reagent (Invitrogen) according to the manufacturer's protocol with PPRE1-pGL3⁴⁹ and pRL-SV40 (Promega). Five hours after transfection, medium was changed to Opti-MEM supplemented with penicillin (100 U/mL), streptomycin (100 μ g/mL), and additionally containing 0.1 % DMSO and the respective test compound or 0.1 % DMSO alone as untreated control. Each concentration was tested in duplicates and each experiment was repeated independently at least three times. After overnight (14–16 h) incubation the cells were assayed

for luciferase activity using the Dual-Glo Luciferase Assay System (Promega) according to the manufacturer's protocol. Luminescence was measured with a Tecan Spark luminometer (Tecan Deutschland GmbH). Normalization of transfection efficiency and cell growth was done by division of firefly luciferase data by *Renilla* luciferase data and multiplying the value by 1000 resulting in relative light units (RLU). Fold activation was obtained by dividing the mean RLU of test compound by the mean RLU of the untreated control. The PPRE reporter gene assay was validated with rosiglitazone as PPAR γ reference agonist which yielded an EC₅₀ value in agreement with the literature. Characterization of *cis*-**AzoRosi-4** was performed in the same way with pre-irradiated compound (irradiation for 3 min at λ = 365 nm right before incubation). To maintain the compound in *cis*-adapted state, the Cell Disco System was used during incubation with 75 ms light pulses (λ = 370 nm) every 15 s.

Production of recombinant PPAR γ LBD protein

Cloning of PPAR γ LBD. A cDNA sequence optimized for codon usage in E.coli K12 and coding for an N-terminal His₁₀-tag followed in frame by a TEV cleavage site and the PPAR γ LBD (aa 234–505) was cloned into the backbone of pET29b for expression under the control of the T7 promoter.

Protein Expression. E.coli BL21 DE3 was transformed with the described expression plasmid and the plasmid pGro7 for co-expression of GroEL/ES (chaperone plasmid set; TaKaRa Bio, Inc.). Cultures in LB medium containing 35 μ g/mL kanamycin and 34 μ g/mL chloramphenicol were grown at 37°C and 180 rpm. When OD₆₀₀ reached 0.6 - 0.7 the temperature was lowered to 18°C and expression of GroEL/ES was induced by addition of 1 g/L L-arabinose. 30 minutes later expression of PPAR γ LBD was induced by the addition of 0.5 mM IPTG and the cultures were supplemented with ~200 μ L Antifoam Y-30 (Sigma-Aldrich) per liter. After 14 - 18 h the cells were harvested by centrifugation (20 min, 6000xg, 4°C).

Purification. A cell pellet from 2 L of culture was thawed and resuspended in a total volume of 50 mL of lysis buffer (400 mM NaCl, 25 mM Tris pH 7.8, 20 mM β -mercaptoethanol, 10% w/v glycerol) supplemented with 25 mM imidazole, 2 mM MgSO_4 , 750 Kunitz DNase I, 250 Kunitz RNase A, a spatula tip of lysozyme and one tablet of Roche complete EDTA-free protease inhibitor cocktail. After incubation for 30 minutes on wet ice the slurry was diluted with three volumes of IMAC buffer A (400 mM NaCl, 25 mM NaPi pH 7.8, 20 mM β -mercaptoethanol, 10% w/v glycerol) supplemented with 25 mM imidazole and cell lysis was enforced by passage through a homogenizer at a combined pressure of 1000 psi. The suspension was supplemented with 1 mM ATP and incubated for another 30 min on wet ice. Cell debris was removed by centrifugation (20 min, 16500xg, 4°C) and the supernatant was loaded at a flowrate of 3 mL/min onto a prepacked 5 mL HisTrap FF column (Ge Healthcare) preequilibrated in 95% IMAC buffer A and 5% IMAC buffer B (IMAC buffer A containing 500 mM imidazole). To remove unbound proteins, the column was washed with 15 column volumes of the same buffer at 5 mL/min. PPAR γ LBD was eluted by a linear gradient of 20 - 60% IMAC buffer B and supplemented with His $_7$ -tagged TEV protease (molar ratio of 1:25) for digestion of the His-tag during overnight dialysis against a volume of IMAC buffer A sufficient to reduce imidazole to 10 –15 mM. The mixture was run gravity flow through a column packed with 10 mL Ni Sepharose 6 Fast Flow (Ge Healthcare) and the flow through was concentrated under 2 bar pressure from nitrogen gas in an amicon stirring cell equipped with a 10.000 MWCO membrane. 5 mL concentrate were separated on a HiLoad 16/600 Superdex 75 pg gel filtration column (Ge Healthcare) equilibrated and run in assay buffer (150 mM KF, 25 mM HEPES pH 7.5, 10 % w/v glycerol, 5 mM DTT) at 1 mL/min. The protein used for isothermal titration experiments was taken from the middle of the peak corresponding to monomeric PPAR γ LBD.

Isothermal titration calorimetry (ITC)

ITC was conducted on a TA Instruments Affinity ITC (TA Instruments, New Castle, Delaware, USA) using recombinant PPAR γ LBD protein dissolved in buffer at pH 7.5 containing 25 mM HEPES, 150 mM KF, 5 mM DTT, 10 % w/v glycerol and 1% DMSO. **AzoRosi-4** was dissolved to a final concentration of 300 μ M in the same buffer, placed into the ITC syringe and titrated to 172 μ L of PPAR γ LBD protein (64 μ M). Characterization of *cis*- **AzoRosi-4** was performed in the same way with pre-irradiated compound (irradiation for 5 min at λ = 365 nm right before titration). The titration was performed at a temperature of 25 °C with a stirring rate of 75 rpm and 31 injections. The first injection had a reduced volume of 1.0 μ L, followed by 30 injections of 2.5 μ L. An interval of 300 s was maintained between injections. ITC raw data were analysed using NanoAnalyze software package (version 3.7.5). An independent binding model was used to fit the reaction enthalpy (ΔH), binding affinity constant (K_D), and stoichiometry (n). Free energy change (ΔG) was calculated from the equation $\Delta G = -RT \ln K$ and the entropy (ΔS) was calculated from $\Delta G = \Delta H - T\Delta S$.

Associated Content

Supporting Information

NMR-spectra and HPLC analysis, further photophysical characterizations, crystallography and ITC data, PDB files of molecular docking, molecular formula strings.

Author Information

Corresponding Author

*merk@pharmchem.uni-frankfurt.de (ORCID <https://orcid.org/0000-0002-5359-8128>);

*dirktrauner@nyu.edu (ORCID <https://orcid.org/0000-0002-6782-6056>);

Author Contributions

#K.H. and S.W. contributed equally to this work

Notes

The authors declare no competing financial interest.

Acknowledgements

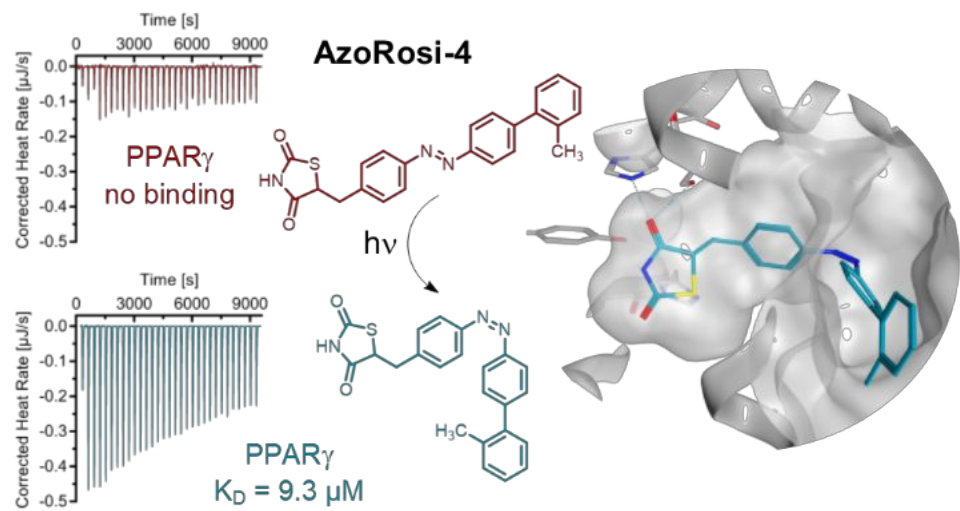
J. M. and K. H. thank the German Academic Scholarship Foundation for a fellowship and J. M. thanks the New York University for a MacCracken fellowship and a Margaret and Herman Sokol fellowship. D.M. is grateful for financial support by the Aventis Foundation. We thank Dr. Lisa Suwandhi and Dr. Siegfried Ussar from Helmholtz Zentrum München for experimental support in the initial stages of the project and Dr. Peter Mayer from LMU for X-ray crystallography data. We thank Boehringer Ingelheim for generous financial support. This work was supported by the National Institutes of Health (Grant R01NS108151-01).

Abbreviations used

NHR, nuclear hormone receptor; RXR, retinoic X receptor; FXR, farnesoid X receptor; ER, estrogen receptor; ChEMBL, chemical database of the European Molecular Biology Laboratory;

IUPHAR, International Union of Basic and Clinical Pharmacology; AF-2, activation function 2; LBD, ligand binding domain; PSS, photostationary state; PPRE, PPAR response element.

Table of Contents graphic



References

- (1) Aranda, A.; Pascual, A. Nuclear Hormone Receptors and Gene Expression. *Physiol. Rev.* **2001**, *81* (3), 1269–1304. <https://doi.org/10.1152/physrev.2001.81.3.1269>.
- (2) Mangelsdorf, D. J.; Thummel, C.; Beato, M.; Herrlich, P.; Schütz, G.; Umesono, K.; Blumberg, B.; Kastner, P.; Mark, M.; Chambon, P.; Evans, R. M. The Nuclear Receptor Superfamily: The Second Decade. *Cell* **1995**, *83* (6), 835–839. [https://doi.org/10.1016/0092-8674\(95\)90199-X](https://doi.org/10.1016/0092-8674(95)90199-X).
- (3) Evans, R. M.; Mangelsdorf, D. J. Nuclear Receptors, RXR, and the Big Bang. *Cell* **2014**, *157* (1), 255–266. <https://doi.org/10.1016/j.cell.2014.03.012>.
- (4) Gronemeyer, H.; Gustafsson, J.-Å.; Laudet, V. Principles for Modulation of the Nuclear Receptor Superfamily. *Nat. Rev. Drug Discov.* **2004**, *3* (11), 950–964. <https://doi.org/10.1038/nrd1551>.
- (5) Ehrmann, J.; Vavrusova, N.; Collan, Y.; Kolar, Z. Peroxisome Proliferator-Activated Receptors (PPARs) in Health and Disease. *Biomed. Pap.* **2002**, *146* (2), 11–14. <https://doi.org/10.5507/bp.2002.002>.
- (6) Nolte, R. T.; Wisely, G. B.; Westin, S.; Cobb, J. E.; Lambert, M. H.; Kurokawa, R.; Rosenfeld, M. G.; Willson, T. M.; Glass, C. K.; Milburn, M. V. Ligand Binding and Co-Activator Assembly of the Peroxisome Proliferator-Activated Receptor- γ . *Nature* **1998**, *395* (6698), 137–143. <https://doi.org/10.1038/25931>.
- (7) Katsouri, L.; Blondrath, K.; Sastre, M. Peroxisome Proliferator-Activated Receptor- γ Cofactors in Neurodegeneration. *IUBMB Life* **2012**, *64* (12), 958–964. <https://doi.org/10.1002/iub.1097>.
- (8) Villapol, S. Roles of Peroxisome Proliferator-Activated Receptor Gamma on Brain and Peripheral Inflammation. *Cell. Mol. Neurobiol.* **2018**, *38* (1), 121–132. <https://doi.org/10.1007/s10571-017-0554-5>.
- (9) Chen, Y.-C.; Wu, J.-S.; Tsai, H.-D.; Huang, C.-Y.; Chen, J.-J.; Sun, G. Y.; Lin, T.-N. Peroxisome Proliferator-Activated Receptor Gamma (PPAR- γ) and Neurodegenerative Disorders. *Mol. Neurobiol.* **2012**, *46* (1), 114–124. <https://doi.org/10.1007/s12035-012-8259-8>.
- (10) Momose, N. C. and Y. Peroxisome Proliferator-Activated Receptor γ Agonists as Insulin Sensitizers: From the Discovery to Recent Progress. *Current Topics in Medicinal Chemistry* **2008**, *8* (17), 1483–1507..
- (11) Kvandová, M.; Majzúnová, M.; Dovinová, I. The Role of PPAR γ in Cardiovascular Diseases. **2016**, *65*, 21.
- (12) Vella, V.; Nicolosi, M. L.; Giuliano, S.; Bellomo, M.; Belfiore, A.; Malaguarnera, R. PPAR- γ Agonists As Antineoplastic Agents in Cancers with Dysregulated IGF Axis. *Front. Endocrinol.* **2017**, *8*. <https://doi.org/10.3389/fendo.2017.00031>.
- (13) Koeffler, H. P. Peroxisome Proliferator-Activated Receptor γ and Cancers. *Clinical Cancer Research* **2003**, *9* (1), 1-9.
- (14) Dhiman, V. K.; Bolt, M. J.; White, K. P. Nuclear Receptors in Cancer — Uncovering New and Evolving Roles through Genomic Analysis. *Nat. Rev. Genet.* **2018**, *19* (3), 160–174. <https://doi.org/10.1038/nrg.2017.102>.
- (15) Broichhagen, J.; Frank, J. A.; Trauner, D. A Roadmap to Success in Photopharmacology. *Acc. Chem. Res.* **2015**, *48* (7), 1947–1960. <https://doi.org/10.1021/acs.accounts.5b00129>.
- (16) Reversible Photocontrol of Biological Systems by the Incorporation of Molecular Photoswitches. *Chemical Reviews* **2013**, *113* (8), 6114–6178. <https://pubs.acs.org/doi/10.1021/cr300179f>.
- (17) Hüll, K.; Morstein, J.; Trauner, D. In Vivo Photopharmacology. *Chem. Rev.* **2018**, *118* (21), 10710–10747. <https://doi.org/10.1021/acs.chemrev.8b00037>.
- (18) Beharry, A. A.; Wong, L.; Tropepe, V.; Woolley, G. A. Fluorescence Imaging of Azobenzene Photoswitching In Vivo. *Angew. Chem. Int. Ed.* **2011**, *50* (6), 1325–1327. <https://doi.org/10.1002/anie.201006506>.
- (19) Morstein, J.; Hill, R. Z.; Novak, A. J. E.; Feng, S.; Norman, D. D.; Donthamsetti, P. C.; Frank, J. A.; Harayama, T.; Williams, B. M.; Parrill, A. L.; Tigyi, G. J.; Riezman, H.; Isacoff, E. Y.; Bautista, D. M.; Trauner, D. Optical Control of Sphingosine-1-Phosphate Formation and Function. *Nat. Chem. Biol.* **2019**, *15* (6), 623–631. <https://doi.org/10.1038/s41589-019-0269-7>.
- (20) Frank, J. A.; Yushchenko, D. A.; Hodson, D. J.; Lipstein, N.; Nagpal, J.; Rutter, G. A.; Rhee, J.-S.; Gottschalk, A.; Brose, N.; Schultz, C.; Trauner, D. Photoswitchable Diacylglycerols Enable Optical Control of Protein Kinase C. *Nat. Chem. Biol.* **2016**, *12* (9), 755–762. <https://doi.org/10.1038/nchembio.2141>.

- (21) Frank, J. A.; Yushchenko, D. A.; Fine, N. H. F.; Duca, M.; Citir, M.; Broichhagen, J.; Hodson, D. J.; Schultz, C.; Trauner, D. Optical Control of GPR40 Signalling in Pancreatic β -Cells. *Chem. Sci.* **2017**, *8* (11), 7604–7610. <https://doi.org/10.1039/C7SC01475A>.
- (22) Frank, J. A.; Moroni, M.; Moshourab, R.; Sumser, M.; Lewin, G. R.; Trauner, D. Photoswitchable Fatty Acids Enable Optical Control of TRPV1. *Nat. Commun.* **2015**, *6* (1), 1–11. <https://doi.org/10.1038/ncomms8118>.
- (23) Frank, J. A.; Franquelim, H. G.; Schwille, P.; Trauner, D. Optical Control of Lipid Rafts with Photoswitchable Ceramides. *J. Am. Chem. Soc.* **2016**, *138* (39), 12981–12986. <https://doi.org/10.1021/jacs.6b07278>.
- (24) Optical manipulation of sphingolipid biosynthesis using photoswitchable ceramides. *eLife* **2019**, <https://doi.org/10.7554/eLife.43230.001>.
- (25) Leinders-Zufall, T.; Storch, U.; Bleymehl, K.; Mederos y Schnitzler, M.; Frank, J. A.; Konrad, D. B.; Trauner, D.; Gudermann, T.; Zufall, F. PhoDAGs Enable Optical Control of Diacylglycerol-Sensitive Transient Receptor Potential Channels. *Cell Chem. Biol.* **2018**, *25* (2), 215–223.e3. <https://doi.org/10.1016/j.chembiol.2017.11.008>.
- (26) Lichtenegger, M.; Tiapko, O.; Svobodova, B.; Stockner, T.; Glasnov, T. N.; Schreibmayer, W.; Platzer, D.; Cruz, G. G. de la; Krenn, S.; Schober, R.; Shrestha, N.; Schindl, R.; Romanin, C.; Groschner, K. An Optically Controlled Probe Identifies Lipid-Gating Fenestrations within the TRPC3 Channel. *Nat. Chem. Biol.* **2018**, *14* (4), 396–404. <https://doi.org/10.1038/s41589-018-0015-6>.
- (27) Morstein, J.; Awale, M.; Reymond, J.-L.; Trauner, D. Mapping the Azolog Space Enables the Optical Control of New Biological Targets. *ACS Cent. Sci.* **2019**, *5* (4), 607–618. <https://doi.org/10.1021/acscentsci.8b00881>.
- (28) Morstein, J.; Trads, J. B.; Hinnah, K.; Willems, S.; Barber, D. M.; Trauner, M.; Merk, D.; Trauner, D. Optical Control of the Nuclear Bile Acid Receptor FXR with a Photohormone. *Chem. Sci.* **2020**, *11* (2), 429–434. <https://doi.org/10.1039/C9SC02911G>.
- (29) Tsuchiya, K.; Umeno, T.; Tsuji, G.; Yokoo, H.; Tanaka, M.; Fukuhara, K.; Demizu, Y.; Misawa, T. Development of Photoswitchable Estrogen Receptor Ligands. *Chem. Pharm. Bull. (Tokyo)* **2020**, *68* (4), 398–402. <https://doi.org/10.1248/cpb.c19-01108>.
- (30) Schoenberger, M.; Damijonaitis, A.; Zhang, Z.; Nagel, D.; Trauner, D. Development of a New Photochromic Ion Channel Blocker via Azologization of Fomocaine. *ACS Chem. Neurosci.* **2014**, *5* (7), 514–518. <https://doi.org/10.1021/cn500070w>.
- (31) Proschak, E.; Heitel, P.; Kalinowsky, L.; Merk, D. Opportunities and Challenges for Fatty Acid Mimetics in Drug Discovery. *J. Med. Chem.* **2017**, *60* (13), 5235–5266. <https://doi.org/10.1021/acs.jmedchem.6b01287>.
- (32) Pirat, C.; Farce, A.; Lebègue, N.; Renault, N.; Furman, C.; Millet, R.; Yous, S.; Specia, S.; Berthelot, P.; Desreumaux, P.; Chavatte, P. Targeting Peroxisome Proliferator-Activated Receptors (PPARs): Development of Modulators. *J. Med. Chem.* **2012**, *55* (9), 4027–4061. <https://doi.org/10.1021/jm101360s>.
- (33) Frkic, R. L.; He, Y.; Rodriguez, B. B.; Chang, M. R.; Kuruvilla, D.; Ciesla, A.; Abell, A. D.; Kamenecka, T. M.; Griffin, P. R.; Bruning, J. B. Structure–Activity Relationship of 2,4-Dichloro- *N*-(3,5-Dichloro-4-(Quinolin-3-Yloxy)Phenyl)Benzenesulfonamide (INT131) Analogs for PPAR γ -Targeted Antidiabetics. *J. Med. Chem.* **2017**, *60* (11), 4584–4593. <https://doi.org/10.1021/acs.jmedchem.6b01727>.
- (34) Giampietro, L.; D'Angelo, A.; Giancrisofaro, A.; Ammazalorso, A.; De Filippis, B.; Fantacuzzi, M.; Linciano, P.; Maccallini, C.; Amoroso, R. Synthesis and Structure–Activity Relationships of Fibrate-Based Analogues inside PPARs. *Bioorg. Med. Chem. Lett.* **2012**, *22* (24), 7662–7666. <https://doi.org/10.1016/j.bmcl.2012.09.111>.
- (35) Nevin, D. K.; Peters, M. B.; Carta, G.; Fayne, D.; Lloyd, D. G. Integrated Virtual Screening for the Identification of Novel and Selective Peroxisome Proliferator-Activated Receptor (PPAR) Scaffolds. *J. Med. Chem.* **2012**, *55* (11), 4978–4989. <https://doi.org/10.1021/jm300068n>.
- (36) Jang, J. Y.; Bae, H.; Lee, Y. J.; Choi, Y. I.; Kim, H. J.; Park, S. B.; Suh, S. W.; Kim, S. W.; Han, B. W. Structural Basis for the Enhanced Anti-Diabetic Efficacy of Lobeglitazone on PPAR Gamma. *Sci Rep* **2018**, *8*, 31–31. <https://doi.org/10.2210/pdb5ycp/pdb>.
- (37) PPAR Gamma LBD Complexed with the Agonist GW1929 (PDB 6D8X), DOI:10.2210/Pdb6D8X/Pdb.
- (38) *Molecular Operating Environment (MOE), Version 2018.0101, Chemical Computing Group Inc. Montreal, QC, Canada.*

- (39) Henke, B. R.; Blanchard, S. G.; Brackeen, M. F.; Brown, K. K.; Cobb, J. E.; Collins, J. L.; Harrington, W. Wallace; Hashim, M. A.; Hull-Ryde, E. A.; Kaldor, I.; Kliewer, S. A.; Lake, D. H.; Leesnitzer, L. M.; Lehmann, J. M.; Lenhard, J. M.; Orband-Miller, L. A.; Miller, J. F.; Mook, Robert A.; Noble, S. A.; Oliver, William; Parks, D. J.; Plunket, K. D.; Szewczyk, J. R.; Willson, T. M. N-(2-Benzoylphenyl)-L-Tyrosine PPAR γ Agonists. 1. Discovery of a Novel Series of Potent Antihyperglycemic and Antihyperlipidemic Agents. *J. Med. Chem.* **1998**, *41* (25), 5020–5036. <https://doi.org/10.1021/jm9804127>.
- (40) Lehmann, J. M.; Moore, L. B.; Smith-Oliver, T. A.; Wilkison, W. O.; Willson, T. M.; Kliewer, S. A. An Antidiabetic Thiazolidinedione Is a High Affinity Ligand for Peroxisome Proliferator-Activated Receptor γ (PPAR γ). *J. Biol. Chem.* **1995**, *270* (22), 12953–12956. <https://doi.org/10.1074/jbc.270.22.12953>.
- (41) Zidar, N.; Tomašić, T.; Šink, R.; Rupnik, V.; Kovač, A.; Turk, S.; Patin, D.; Blanot, D.; Contreras Martel, C.; Dessen, A.; Müller Premru, M.; Zega, A.; Gobec, S.; Peterlin Mašič, L.; Kikelj, D. Discovery of Novel 5-Benzylidenetherodanine and 5-Benzylidenethiazolidine-2,4-Dione Inhibitors of MurD Ligase. *J. Med. Chem.* **2010**, *53* (18), 6584–6594. <https://doi.org/10.1021/jm100285g>.
- (42) Liu, C.; Feng, T.; Zhu, N.; Liu, P.; Han, X.; Chen, M.; Wang, X.; Li, N.; Li, Y.; Xu, Y.; Si, S. Identification of a Novel Selective Agonist of PPAR γ with No Promotion of Adipogenesis and Less Inhibition of Osteoblastogenesis. *Sci. Rep.* **2015**, *5* (1), 9530. <https://doi.org/10.1038/srep09530>.
- (43) Borowiak, M.; Nahaboo, W.; Reynders, M.; Nekolla, K.; Jalinot, P.; Hasserodt, J.; Rehberg, M.; Delattre, M.; Zahler, S.; Vollmar, A.; Trauner, D.; Thorn-Seshold, O. Photoswitchable Inhibitors of Microtubule Dynamics Optically Control Mitosis and Cell Death. *Cell* **2015**, *162* (2), 403–411. <https://doi.org/10.1016/j.cell.2015.06.049>.
- (44) Diabetes Drug Affects the Brain. *Nature* **2011**, *473* (7345), 9–9. <https://doi.org/10.1038/473009e>.
- (45) Cao, J.; Ou, G.; Yang, N.; Ding, K.; Kream, B. E.; Hamrick, M. W.; Isales, C. M.; Shi, X. M. Impact of Targeted PPAR γ Disruption on Bone Remodeling. *Mol. Cell. Endocrinol.* **2015**, *410*, 27–34. <https://doi.org/10.1016/j.mce.2015.01.045>.
- (46) Lerch, M. M.; Hansen, M. J.; van Dam, G. M.; Szymanski, W.; Feringa, B. L. Emerging Targets in Photopharmacology. *Angew. Chem. Int. Ed.* **2016**, *55* (37), 10978–10999. <https://doi.org/10.1002/anie.201601931>.
- (47) Morstein, J.; Trauner, D. New Players in Phototherapy: Photopharmacology and Bio-Integrated Optoelectronics. *Curr. Opin. Chem. Biol.* **2019**, *50*, 145–151. <https://doi.org/10.1016/j.cbpa.2019.03.013>.
- (48) Rau, O.; Wurglics, M.; Paulke, A.; Zitzkowski, J.; Meindl, N.; Bock, A.; Dingermaier, T.; Abdel-Tawab, M.; Schubert-Zsilavecz, M. Carnosic Acid and Carnosol, Phenolic Diterpene Compounds of the Labiate Herbs Rosemary and Sage, Are Activators of the Human Peroxisome Proliferator-Activated Receptor Gamma. *Planta Med.* **2006**, *72* (10), 881–887. <https://doi.org/10.1055/s-2006-946680>.
- (49) Pollinger, J.; Gellrich, L.; Schierle, S.; Kilu, W.; Schmidt, J.; Kalinowsky, L.; Ohrndorf, J.; Kaiser, A.; Heering, J.; Proschak, E.; Merk, D. Tuning Nuclear Receptor Selectivity of Wy14,643 towards Selective Retinoid X Receptor Modulation. *J. Med. Chem.* **2019**, *62* (4), 2112–2126. <https://doi.org/10.1021/acs.jmedchem.8b01848>.
- (50) Agilent (2014). *CrysAlis PRO*. Agilent Technologies Ltd, Yarnton, Oxfordshire, England.
- (51) Altomare, A.; Burla, M. C.; Camalli, M.; Cascarano, G. L.; Giacovazzo, C.; Guagliardi, A.; Moliterni, A. G. G.; Polidori, G.; Spagna, R. SIR97: A New Tool for Crystal Structure Determination and Refinement. *J. Appl. Crystallogr.* **1999**, *32* (1), 115–119. <https://doi.org/10.1107/S0021889898007717>.
- (52) Sheldrick, G. M. SHELXT – Integrated Space-Group and Crystal-Structure Determination. *Acta Crystallogr. Sect. Found. Adv.* **2015**, *71* (1), 3–8. <https://doi.org/10.1107/S2053273314026370>.
- (53) Farrugia, L. J. WinGX and ORTEP for Windows: An Update. *J. Appl. Crystallogr.* **2012**, *45* (4), 849–854. <https://doi.org/10.1107/S0021889812029111>.
- (54) Bruker (2012). SAINT. Bruker AXS Inc., Madison, Wisconsin, USA.
- (55) Sheldrick, G. M. (1996). SADABS. University of Göttingen, Germany.